

1 **Genome editing in the mouse brain with minimally immunogenic Cas9 RNPs**

2  
3 Elizabeth C. Stahl<sup>1-3</sup>, Jennifer K. Sabo<sup>1\*</sup>, Min Hyung Kang<sup>1,5</sup>, Ryan Allen<sup>1</sup>, Elizabeth Applegate<sup>1</sup>,  
4 Shin Eui Kim<sup>1</sup>, Mika Kwon<sup>1,3</sup>, Anmol Seth<sup>1,3</sup>, Nicholas Lemus<sup>1,3</sup>, Viviana Salinas-Rios<sup>1</sup>,  
5 Katarzyna Soczek<sup>1-3</sup>, Marena Trinidad<sup>1</sup>, Linda T. Vo<sup>1#</sup>, Chris Jeans<sup>2</sup>, Anna Wozniak<sup>4</sup>, Timothy  
6 Morris<sup>4</sup>, Athen Kimberlin<sup>4</sup>, Thomas Foti<sup>4</sup>, David F. Savage<sup>1,3,5</sup> and Jennifer A. Doudna<sup>1-3,5-8†</sup>

7  
8  
9 <sup>1</sup>Innovative Genomics Institute, University of California, Berkeley, California 94720, USA;

10 <sup>2</sup>California Institute for Quantitative Biosciences (QB3), University of California, Berkeley,  
11 California 94720, USA; <sup>3</sup>Department of Molecular and Cell Biology, University of California,  
12 Berkeley, California 94720, USA; <sup>4</sup>Aldevron LLC, Madison, Wisconsin 53719, USA; <sup>5</sup>Howard  
13 Hughes Medical Institute, University of California, Berkeley, California 94720, USA; <sup>6</sup>Department  
14 of Chemistry, University of California, Berkeley, CA, USA 94720; <sup>7</sup>MBIB Division, Lawrence  
15 Berkeley National Laboratory, Berkeley, California 94720, USA; <sup>8</sup>Gladstone Institutes, University  
16 of California, San Francisco, CA 94114

17  
18

19 †Correspondence: [doudna@berkeley.edu](mailto:doudna@berkeley.edu)

20

21 \*Current address: Scribe Therapeutics Inc. Alameda, CA, 94501

22 #Current address: Third Rock Ventures, Boston, MA, 02116

23

24 **Abstract**

25           Transient delivery of CRISPR-Cas9 ribonucleoproteins (RNPs) into the central nervous  
26 system (CNS) for therapeutic genome editing could avoid limitations of viral vector-based delivery  
27 including cargo capacity, immunogenicity, and cost. Here we tested the ability of cell penetrant  
28 Cas9 RNPs to edit the mouse striatum when introduced using a convection enhanced delivery  
29 system. These transient Cas9 RNPs showed greater local editing of neurons and reduced  
30 adaptive immune responses relative to Cas9 delivered using AAV serotype 9. The production of  
31 ultra-low-endotoxin Cas9 protein manufactured at scale further improved innate immunity. We  
32 conclude that injection-based delivery of minimally immunogenic CRISPR genome editing RNPs  
33 into the CNS provides a valuable alternative to virus-mediated genome editing.

34

## 35 Introduction

36 Editing somatic cells directly *in vivo* is anticipated to be the next wave of therapeutics for  
37 many genetic diseases, especially those affecting the central nervous system (CNS)<sup>1,2</sup>. Clustered  
38 regularly interspaced short palindromic repeats (CRISPR) is a revolutionary tool adapted from  
39 bacterial immune systems for genome editing<sup>3-5</sup>. To achieve gene disruption, the functional  
40 endonuclease, Cas9, is directed by a guide RNA to a target site in DNA to generate a double  
41 strand break leading to insertions and deletions (indels). Unfortunately, despite many genetic  
42 disease indications, the brain remains a challenging target for genome editing.

43 To circumvent the blood-brain barrier (BBB), most genomic medicines rely on direct  
44 intracranial injection of viral vectors encoding the transgene of interest. Viral vectors, such as  
45 recombinant adeno-associated virus (AAV), have had great success in gene therapy and are less  
46 immunogenic than most viral vectors, however, they require re-manufacturing for each target and  
47 are hindered by costly production scale up. Additionally, AAV has a limited DNA packaging  
48 capacity and is associated with immunogenicity in the brain from both the vector and expression  
49 of foreign transgenes<sup>6-9</sup>. Although the brain has been considered an immune-privileged site,  
50 green fluorescent protein can induce a strong inflammatory response and neuronal cell death  
51 three weeks after injection with AAV serotype 9 has been reported<sup>6-9</sup>. Additionally, Cas9-specific  
52 immune responses have been elicited following AAV delivery in mice<sup>10-12</sup> and pre-existing cellular  
53 and humoral immunity to Cas9 and AAVs are documented in humans<sup>13-18</sup>. Despite these  
54 drawbacks, AAVs are the most clinically relevant delivery systems currently in use for the CNS.

55 The development of transient, non-viral delivery systems that can effectively edit neurons  
56 throughout the brain with minimal immunogenicity would greatly facilitate future clinical  
57 applications. Previously, we developed cell penetrating Cas9 ribonucleoproteins (RNPs) capable  
58 of genome editing in mouse neurons both *in vitro* and *in vivo*<sup>19</sup>. To enable self-delivery of the Cas9  
59 RNPs, four repeats of the positively charged Simian vacuolating virus 40 nuclear localization  
60 sequences (SV40-NLS) were fused to the N-terminus along with two repeats to the C-terminus of

61 Cas9, a strategy that was also reported to enable delivery of zinc-finger nucleases<sup>20</sup>. Using a  
62 single guide to turn on the tdTomato reporter from the lox-stop-lox (LSL-Ai9<sup>21</sup>) mouse, we reported  
63 edited striatal volume of approximately 1.5mm<sup>3</sup><sup>19</sup>.

64 Here we report further optimization of cell penetrant Cas9 RNPs, demonstrating efficacy  
65 in human primary cells and improved editing of the mouse striatum using a convection enhanced  
66 delivery CED system. We compared the transient RNP complexes to AAV serotype 9 for Cas9  
67 delivery to the CNS, to measure both editing efficiency and the host immune response. We found  
68 that cell penetrant Cas9-RNPs edited significantly more neurons within a given area than Cas9-  
69 AAVs but were less efficient at diffusing throughout the brain and cerebrospinal fluid. Both groups  
70 elicited humoral responses, but anti-capsid antibodies in the Cas9-AAV group persisted at high  
71 levels out to 90-days and AAV treated brains were associated with significantly elevated *Cd3e*  
72 gene expression at four weeks, suggesting an ongoing adaptive immune response. Cas9-RNP  
73 treated brains showed acute microglial activation that was mitigated by reducing endotoxin levels  
74 during protein manufacturing scale up. Studies suggest that correcting pathological mutations in  
75 20-30% of striatal neurons expressing mutant huntingtin protein would be sufficient to significantly  
76 improve the disease pathology<sup>22</sup>. Therefore, Cas9 RNPs are a promising strategy for localized  
77 therapeutic intervention in neurological disorders to address current limitations of viral delivery.



## 78 **Results**

### 79 *Development of Cas9 cell penetrant RNP and AAV to measure genome editing with the* 80 *tdTomato reporter system*

81           Creating a large deletion in the lox-stop-lox cassette in Ai9 mice with a single guide RNA  
82 (sgRNA) enables expression of tdTomato and efficient quantification of editing by fluorescent read  
83 out (Figure S1A). Cas9 from *Streptococcus pyogenes* (engineered with four copies of SV40 NLS  
84 on the N-terminus and two copies on the C-terminus (4x-SpyCas9-2x) to be cell penetrant) was  
85 first produced from recombinant *E. coli* in a laboratory setting, using a low-endotoxin method.  
86 Editing efficiency of the RNP was compared to Cas9 delivered by recombinant adeno-associated  
87 virus (AAV) (Figure 1A-B). Since SpyCas9 cannot fit within a single AAV with its guide RNA, we  
88 used clinically relevant AAV-SauCas9-sgRNA (derived from *Staphylococcus aureus*)<sup>23-25</sup>. AAV  
89 serotype 9 was produced using a baculovirus transfected into Sf9 insect cells<sup>26,27</sup>. To control for  
90 differences in the Cas9 orthologues, cell penetrant 4x-SauCas9-2x protein was also produced  
91 following the same expression and purification methods as 4x-SpyCas9-2x. Due to differences in  
92 PAM requirements between the two Cas9 orthologues (SpyCas9 NGG, SauCas9 NNGRRT), a  
93 new guide was designed for SauCas9 to target the tdTomato locus (Figure S1B).

94           We confirmed editing in neural precursor cells (NPCs) isolated from embryonic day 13.5  
95 Ai9 mice with all constructs *in vitro* (Figure S1C-E). Interestingly, we observed greater editing of  
96 mouse NPCs with SauCas9 when delivered as cell penetrant RNP compared to AAV, as AAV  
97 preps often include empty capsids (Figure S1F) and require high multiplicity of infection for  
98 efficient transduction in cell culture<sup>28,29</sup>. The 4x-SauCas9-2x was slightly less efficacious when  
99 editing mouse NPCs compared to 4x-SpyCas9-2x, which could be explained in part by differences  
100 in the guide RNAs.

101           To further examine the potential for cell penetrant Cas9 RNPs to edit difficult cells *in vitro*,  
102 we tested delivery and editing with 4x-SpyCas9-2x in human neural precursor cells derived from  
103 induced pluripotent stem cells (iPSCs)<sup>30-32</sup>. Human NPCs were treated with pre-formed RNPs

104 using an established guide RNA targeting EMX1<sup>33</sup>. In human cells, we detected 10x higher rates  
105 of editing with 4x-SpyCas9-2x compared to standard RNP delivered with commercial transfection  
106 reagents (Figure S2A-B).

107  
108 *Cas9 RNPs result in modest editing of brain parenchyma following delivery into cerebrospinal*  
109 *fluid*

110 To determine the optimal route of delivery for Cas9 RNPs into the mouse CNS, we tested  
111 intraparenchymal injections into the striatum, as well as injection into the cerebrospinal fluid  
112 (CSF), including intrathecal (IT) and intracerebroventricular (ICV) routes. Following IT injection of  
113 cell penetrant RNPs, we observed edited glial cells and neurons in the cortex and striatum of one  
114 hemisphere, but no editing within the spinal cord (Figure S3A). Following ICV injection of Cas9  
115 RNPs in neonatal p0 mice, we observed tdTomato<sup>+</sup> cells in the subventricular zone and white  
116 matter, including glial cells and neural stem/progenitor cells expressing Ki67 and DCX evaluated  
117 three weeks after delivery (Figure S3B-C). Editing post-ICV injection in adult mice was restricted  
118 to the cells within the lateral ventricles, choroid plexus, subventricular zone, and hippocampus in  
119 a subset of mice (Figure S3D). In all cases, the total number of edited cells with RNP delivery into  
120 the CSF was lower than with direct intraparenchymal injection.

121 Therefore, we sought to further improve upon intraparenchymal injections using a  
122 convection enhanced delivery system (CED), which consists of silicon tubing fused into a blunt  
123 needle to create a cannulated step (Figure S4A). CED has been reported to increase the diffusion  
124 of molecules in the brain, including AAV, which is particularly important in large animal models  
125 and humans<sup>34,35</sup>. While CED did not significantly improve the volume of edited striatal tissue  
126 compared to the non-cannulated blunt needle with 4x-SpyCas9-2x RNP (Figure S4B), CED did  
127 significantly reduce reflux of RNP from the needle-injection track (Figure 1D). Furthermore,  
128 tdTomato<sup>+</sup> neurons edited by Cas9-RNPs within the striatum were observed to extend along the

129 basal ganglia circuit into the globus pallidus and substantia nigra along the anterior-posterior axis  
130 (Figure 1C-E).

131

132 *Convection enhanced delivery of Cas9 RNPs and AAVs mediates robust editing in the mouse*  
133 *striatum*

134 Using bilateral CED injections into the striatum, we compared edited tissue volume using  
135 the 4x-SpyCas9-2x RNP, 4x-SauCas9-2x RNP, and AAV9-SauCas9-sgRNA in adult Ai9 mice at  
136 three weeks post-injection. Despite performing well *in vitro*, 4x-SauCas9-2x RNPs  
137 underperformed *in vivo* when tested at two different doses and additional NLS configurations  
138 (Figure S5). Therefore, we performed our primary comparison between 4x-SpyCas9-2x RNP  
139 (hereafter referred to as Cas9-RNP) and AAV9-SauCas9-sgRNA (hereafter referred to as Cas9-  
140 AAV).

141 Overall, we observed diffuse tdTomato signal throughout the striatum and cortex in the  
142 Cas9-AAV group, whereas we observed more intense tdTomato signal emanating from the  
143 injection site with the Cas9-RNP group (Figure 1F, Figure S6C). We tested several doses of Cas9-  
144 RNP by keeping the injection volume constant and increasing the concentration of the RNP in  
145 solution from 10 $\mu$ M to 100 $\mu$ M. There was no significant difference in the edited striatal volume  
146 when delivering RNPs in this concentration range (Figure 1H) and editing levels seemed to  
147 decrease slightly at 50 $\mu$ M and 100 $\mu$ M compared to the 10 $\mu$ M and 25 $\mu$ M groups. We chose the  
148 25 $\mu$ M concentration (4.15 mg/mL or approximately 1.75 mg/kg Cas9) group for further study as it  
149 had the highest maximal editing rate. Above 25 $\mu$ M in the RNP group, we observed a decrease in  
150 NeuN staining and an increase in GFAP staining out to 90-days in the Cas9-RNP group,  
151 suggesting dose-limiting effects (Figure 1G).

152 At both 21 and 90-days post-injection, the Cas9-AAV group outperformed the Cas9-RNP  
153 group when quantifying total edited striatal volume (n=8 at 21-days, n=4 at 90-days, p<0.05,

154 Figure 1I). The volume of edited cells was relatively stable in the Cas9-AAV group between 21  
155 and 90-days at approximately  $47 \pm 3\%$  (covering approximately  $13.4 \text{ mm}^3$  of striatum), while the  
156 Cas9-RNP group had editing levels of  $22 \pm 3\%$  (approximately  $6.2 \text{ mm}^3$  of striatum) between 21  
157 and 90-days (increased from previous report of editing  $1.5 \text{ mm}^3$  striatal volume<sup>19</sup>). Edited cells  
158 were observed further along the rostral-caudal axis ( $-2.12 \text{ mm}$  to  $2.5 \text{ mm}$  relative to Bregma),  
159 demonstrating better diffusion of the editor away from the injection site in the Cas9-AAV group  
160 (Figure S6D-E).

161 Since large deletions in the tdTomato locus make on-target editing difficult to assess using  
162 short-read next-generation sequencing (NGS), we developed an NHEJ droplet digital PCR assay  
163 (ddPCR) to measure drop-off of HEX-labeled probes over the cut sites, in relation to distal  
164 reference FAM-labeled probes. Genomic DNA was isolated from 2-mm thick sections of each  
165 injected hemisphere, covering multiple brain sub-structures. Loss of the HEX probe reached  $2 \pm$   
166  $1\%$  in the Cas9-RNP group and  $15 \pm 10\%$  in the Cas9-AAV group, indicating edited alleles, when  
167 measured at 28-days (Figure S5G).

168 We also quantified the percentage of edited NeuN<sup>+</sup> neurons within the tdTomato<sup>+</sup> region  
169 of interest (ROI) per hemisphere between Cas9-AAV and Cas9-RNP at the 21-day timepoint. We  
170 found that Cas9-RNP edited significantly more NeuN<sup>+</sup> neurons per ROI ( $36 \pm 10\%$ ) compared to  
171 Cas9-AAV ( $20 \pm 2\%$ ) (Figure 1J,  $n=6-8$  injections,  $p<0.05$ ). Within the ROI, neurons were the  
172 most frequently edited cell type in both groups, including DARPP32<sup>+</sup> medium spiny neurons  
173 (Figure S6). Additionally editing of ALDH1L1<sup>+</sup> and OLIG2<sup>+</sup> glial cells was noted in both groups  
174 (approximately 2% of edited cells within the ROI in the Cas9-RNP group and 8% of cells in the  
175 Cas9-AAV group). Therefore, Cas9-RNPs generated higher rates of edited neurons within a given  
176 area and demonstrated a preference for editing neurons over glial cells, as observed previously<sup>19</sup>,  
177 compared to Cas9-AAV (Figure S6A-B).

178

179 *Comparison of local and peripheral immune response between Cas9 RNPs and AAVs in the Ai9*  
180 *reporter mouse*

181 We next examined the local and peripheral immune response following delivery of Cas9  
182 RNPs and AAVs into the brain. Using immunofluorescent staining for Iba1 (Figure 2A), we  
183 observed similar numbers of microglia between the groups, but increased staining intensity in the  
184 25 $\mu$ M Cas9-RNP group leading to a significant increase in percent Iba1<sup>+</sup> area from sham-treated  
185 animals (Figure 2B, n=6 replicates, one-way ANOVA, p<0.05). Staining for CD45 showed dim  
186 expression on Iba1<sup>+</sup> microglia and high expression on CD3<sup>+</sup> T-cells, which were slightly increased  
187 in the 25 $\mu$ M Cas9-RNP group compared to the sham and Cas9-AAV, but not significant different,  
188 at three weeks post-injection (Figure 2C-D, n=6-12 replicates).

189 In addition to the immune response at the local site of injection, circulating IgG antibodies  
190 were measured at 28 and 90-days post-injection. We found that sham-treated animals had no  
191 pre-existing antibodies to either SpyCas9, SauCas9, nor AAV9 capsids. At 28-days following  
192 striatal injection, there was a 1.6e4-fold increase in anti-SpyCas9 IgG in the 25 $\mu$ M Cas9-RNP  
193 group, a 1.3e4-fold increase in anti-AAV9 capsid IgG in the Cas9-AAV group, and an 8.9e1-fold  
194 increase in anti-SauCas9 IgG in the Cas9-AAV group (i.e., humoral response against transgene)  
195 (Figure 2E, n=3-5 biological replicates). No cross-reactivity was observed between orthologue  
196 RNPs, as described previously<sup>11</sup>, nor were any anti-AAV capsid antibodies detected in the RNP  
197 group. At 90-days, the levels of IgG fell to a 5.4e2-fold increase in the 25 $\mu$ M Cas9 RNP group  
198 and 1.2e4-fold increase in the Cas9 AAV group from the sham controls, demonstrating greater  
199 maintenance of systemic antibodies against the capsid in the AAV group.

200 The cellular and humoral immune response to Cas9 RNPs was dose-dependent and a  
201 significant increase in CD45<sup>+</sup> cells was observed at the 100 $\mu$ M RNP dose compared to sham,  
202 Cas9-AAV, and Cas9-RNP at 25 $\mu$ M (Figure S7). Cas9-reactive cells were also identified in the

203 spleen by interferon-gamma (IFN- $\gamma$ ) ELISpot assay (Figure S7E) at both 25 $\mu$ M and 100 $\mu$ M doses  
204 of Cas9-RNPs, but not in sham treated animals.

205         Since the mice had no pre-existing antibodies to SpyCas9, we tested how the immune  
206 response would differ in the RNP group by first exposing the mice to a single subcutaneous  
207 injection of 4x-SpyCas9-2x protein and adjuvant (AddaVax<sup>TM</sup>) four-weeks prior to stereotaxic  
208 surgery with Cas9-RNPs. We found that pre-exposing the mice to Cas9 had a synergistic effect  
209 on both serum IgG and activation of IFN- $\gamma$ <sup>+</sup> cells in the spleen (Figure S7F-I). Mice that received  
210 surgery maintained tdTomato<sup>+</sup> cells in the brain to the measured time point. Additional studies  
211 using this immunization strategy may help to further characterize the immune response to Cas9-  
212 RNPs by modeling pre-existing immunity relevant to humans.

213         Finally, we measured gene expression changes in mice that received Cas9-RNP and AAV  
214 at 3 and 28-days post-injection using RT-qPCR. At three days, the Cas9-AAV group had a modest  
215 but significant increase in *Fas* (1.19-fold) and *Fasl* (1.85-fold) compared to the sham group (Figure  
216 2F). At 28-days post-injection, both Cas9-RNP and -AAV had a significant increase in *Fas* (1.61  
217 and 1.89-fold respectively). In addition, the Cas9-AAV group had a significant increase in *CD3e*  
218 gene expression (5.45-fold, n=4 replicates, p<0.05), closely followed by *CD8a* (2.06-fold, ns,  
219 p=0.06), while Cas9-RNP had a slight but non-significant increase in *CD3e* (2.15-fold, ns, p=0.06),  
220 compared to the sham group.

221         There were no detectable off-target editing events at 1 and 4-months post-injection in any  
222 of the experimental groups at the evaluated off-target sites (Figure S8A-C). In the Cas9-AAV  
223 group, the Cas9 transgene was expressed in the brain out to 4-months, the last tested time point,  
224 as expected (Figure S8D). Additionally, few genes were differentially expressed between the  
225 groups at 4-months, except for *Fas* (1.54-fold), which was significantly elevated in the Cas9-AAV  
226 group compared to the sham (Figure S8E-F). We used long read sequencing to examine whether  
227 any fragments of the viral genome had been integrated near the cut site in the tdTomato locus,

228 as previously reported<sup>36–39</sup>. We also observed partial integrations of viral fragments in our  
229 amplicon, although our *in vivo* editing rates and sequencing depth were relatively low (Figure S9).

230 We concluded that delivery of Cas9 to the brain was well-tolerated in naïve mice. However,  
231 the increase of Iba1<sup>+</sup> cells near tdTomato<sup>+</sup> cells in the striatum in the 25 $\mu$ M Cas9-RNP group  
232 raised the question of whether the response was due to Cas9 itself or impurities within the protein  
233 product. We hypothesized that the local immune response may be due to endotoxins from *E. coli*  
234 in the RNP complexes.

235

### 236 *Production and testing of ultra-low endotoxin 4x-SpyCas9-2x protein*

237 To examine the impact of endotoxin on the immune response to RNPs, we partnered with  
238 a commercial producer of Cas9 protein and were able to significantly scale up manufacturing to  
239 produce a large quantity of ultra-low endotoxin 4x-SpyCas9-2x protein using an industrial tag-free  
240 expression and purification system (Figure 3A).

241 Using the limulus amoebocyte lysate (LAL) assay, we measured an endotoxin  
242 concentration of 0.035 EU/mg in the industrial-produced protein compared to 0.2 EU/mg in the  
243 lab-produced protein (Figure S10A). Interestingly, using the same assay, we found that guide  
244 RNA could be an unexpected source of endotoxin contamination. Endotoxin was present in at  
245 least three unopened vials of lyophilized RNA that had been stored at -80°C from a 2018 lot, but  
246 not in a more recently purchased lot from the same vendor when resuspended simultaneously  
247 (Figure S10A-C). To rule out false positives due to reaction of LAL with beta-glucans, we  
248 performed the Recombinant Factor C (rFC) assay. The guide RNAs had a similar level of  
249 endotoxins between the LAL and rFC assays, demonstrating the positive signal was from  
250 contamination with endotoxin and not beta-glucans (Figure S10D-E).

251 To measure the physiological impact of endotoxin in our samples, we used HEK293 cells  
252 that were engineered to produce secreted embryonic alkaline phosphatase (SEAP) downstream



253 of NF- $\kappa$ B activation resulting from human toll-like receptor 4 stimulation (hTLR4) with  
254 endotoxin/lipopolysaccharide (LPS, Figure S11A-E). The lab-produced protein stimulated NF- $\kappa$ B  
255 in HEK293 cells significantly greater than the industrial produced protein ( $p < 0.01$ , unpaired t-test).  
256 Treatment with the industrially produced protein led to similar levels of SEAP between hTLR4  
257 cells and the parental cell line (Null2), demonstrating that most of the NF- $\kappa$ B stimulation was  
258 downstream of other pattern-recognition receptors (such as TLR3, TLR5, or nucleotide-binding  
259 oligomerization domain-containing protein 1 (NOD-1) activation) and not due to LPS signaling  
260 through hTLR4 (Figure S11A-E). When combined with sg298 from the 2018 or 2022 lot,  
261 absorbance levels of SEAP further increased in RNP complexes made with lab produced protein,  
262 while the industrial protein with either guide did not induce a response (Figure S11F).  
263 Furthermore, guide RNA alone did not stimulate NF- $\kappa$ B in HEK293 cells (Figure S11D).

264 Finally, we measured endotoxins in the “optimized” formulation of RNPs, comprised of the  
265 industrially produced 4x-SpyCas9-2x protein and 2022 sgRNA, using the LAL assay. Estimating  
266 delivery of 10 $\mu$ L per mouse, the endotoxin burden was 0.44 EU/kg when RNPs were formulated  
267 at 25 $\mu$ M. These data suggest that RNPs could be delivered below the 0.2 EU/kg FDA threshold  
268 for intrathecal delivery<sup>40</sup> when formulated at 10 $\mu$ M without significant loss of editing (Figure 3B  
269 and Figure 1H).

270

### 271 *Optimized RNP formulation reduces immune response*

272 We performed CED bilateral intrastriatal injections to test if reducing endotoxins would  
273 improve the host immune response to RNPs *in vivo*. In this experiment, we compared the  
274 optimized RNP formulation (industrially produced 4x-SpyCas9-2x NLS protein with sg298 2022)  
275 to the standard formulation used in Figures 1 and 2 (laboratory produced 4x-SpyCas9-2x NLS  
276 protein with sg298 2018) at 25 $\mu$ M. The standard RNP induced a significant increase in Iba1<sup>+</sup> area,  
277 consistent with our previous measurements (Figure 3C and Figure 1A); however, the optimized



278 Cas9-RNP formulation did not induce microglial activation. Additionally, there was no increase in  
279 CD45<sup>+</sup> and CD3<sup>+</sup> cells from the sham in the optimized RNP group (Figure 3D). Of note, the  
280 standard RNP edited an average of 31 ± 3% striatal volume (greater than values reported in  
281 Figure 1), while the optimized RNP edited an average of 23 ± 8% striatal volume (Figure 3F).  
282 Interestingly, the standard RNP also lead to significantly greater anti-Cas9 IgG responses at  
283 three-weeks post-injection, possibly due to endotoxin boosting the adaptive immune response  
284 (Figure 3G). Taken together, we found that reducing endotoxins in both the guide RNA and protein  
285 components of the RNP leads to a reduced innate immune response, comparable to the sham  
286 and AAV9 groups, while maintaining high on-target editing. Furthermore, cell penetrant Cas9  
287 proteins are more amenable than AAVs for expedited manufacturing of large quantities suitable  
288 for *in vivo* experiments.

289 In conclusion, our results establish complementary genome editing and immunogenicity  
290 outcomes between the two tested Cas9 delivery strategies. To enable editing of multiple sub-  
291 brain structures, glial cells, and delivery through the CSF, AAV serotype 9 is preferred. To enable  
292 high levels of editing in neurons within a localized brain sub-structure, minimizing adaptive  
293 immune responses, and enabling manufacturing scale up, the RNP is preferred.

294

## 295 **Discussion**

296 In the present study, we demonstrate that cell penetrant Cas9 RNPs edit a therapeutically  
297 relevant volume of the mouse striatum using convection enhanced delivery. Furthermore, the 4x-  
298 NLS modification enables self-delivery of Cas9 orthologous proteins *in vitro* to both mouse and  
299 human cells, demonstrating cross-species compatibility of the system for the first time. We also  
300 show that Cas9 RNPs have dose-dependent effects on the immune response, which can be  
301 mitigated by using ultra-low endotoxin protein produced in an industrial non-GMP setting. These  
302 experiments are informative for the design of future therapeutic applications of Cas9 RNP editors  
303 in mice and larger animal models.

304 Several studies have reported non-viral delivery of Cas9 into the mouse brain. The  
305 “CRISPR-Gold” Cas9 nanoparticle delivery system induced 14% edited glial cells near the  
306 injection site, sufficient to reduce repetitive behaviors in a mouse model of fragile X syndrome<sup>41</sup>.  
307 Additionally, incubating RNPs with R7L10, an arginine and leucine rich cationic peptide, induced  
308 45% indels in the CA3 region of the hippocampus, leading to behavioral improvements in an  
309 Alzheimer’s disease mouse model<sup>42</sup>. Furthermore, editing of DARPP-32 medium spiny neurons  
310 in the striatum was achieved using RNPs packaged in biodegradable PEGylated nanocapsules<sup>43</sup>.  
311 Interestingly these nanocapsules had a neutral charge, while our 4x-Cas9-2x NLS RNPs have a  
312 net-positive charge, suggesting the mechanism of entry may differ between the two strategies.

313 Systemic delivery of genome editors with glucose-conjugated silica nanoparticles and  
314 AAV9 can lead to modest levels of editing in the brain, sufficient for therapeutic benefit<sup>44,45</sup>. In  
315 this study, we found that the Cas9-AAV distributed further through the brain than Cas9-RNPs,  
316 although the RNP delivery approach was more effective for high levels of localized neuronal  
317 editing. It is important to note that expression of the tdTomato protein in the Ai9 mouse model  
318 significantly underreports the actual genome editing efficiency, as double strand breaks that result  
319 in small indels are not sufficient to turn on the reporter<sup>19</sup>. Despite the need for direct injection, the  
320 simplicity of the cell penetrant protein makes it ideal from a manufacturing perspective compared  
321 to other nanoparticle formulations. The cell penetrant RNP could be further mixed with polymers,  
322 such as polyethylene glycol (PEG)<sup>46</sup>, to improve biodistribution in the future.

323 We hypothesized that cell penetrant Cas9-RNPs would be less immunogenic than Cas9-  
324 AAVs due to their transient expression. As the dose of 4x-SpyCas9-2x RNPs increased from  
325 25 $\mu$ M to 100 $\mu$ M, there was an increase in CD45<sup>+</sup> and GFAP<sup>+</sup> cells, and a decrease in NeuN<sup>+</sup>  
326 cells. As such, subsequent experiments were performed at 25 $\mu$ M, which was well-tolerated and  
327 resulted in similar levels of editing as the higher dose. The 25 $\mu$ M Cas9-RNP led to lower levels  
328 of vehicle-specific antibodies by 90-days post-injection compared to AAVs and did not upregulate

329 gene signatures of T-cells at 28-days as measured by RT-qPCR, supporting our hypothesis.  
330 Reducing endotoxin in both the Cas9 protein and guide RNA prevented microglial reactions and  
331 reduced humoral responses at 21-days.

332 In the Cas9-AAV group, few immune cells (CD45, Iba1, or CD3) were observed in the  
333 striatum by immunostaining, however *CD3e* gene expression was significantly upregulated in  
334 explanted tissue, closely followed by an increase in *CD8a*. This finding could indicate  
335 accumulation of cytotoxic T-cells trafficking into the parenchyma from the blood vessels or  
336 ventricles. Additionally, no changes in NeuN, GFAP, and CD45 expression were observed in the  
337 Cas9-AAV group out to 4 months, demonstrating that the AAV delivery strategy was well-tolerated  
338 overall in naïve mice. A study by Li et al. found that mice immunized against SauCas9 with  
339 Freund's adjuvant one week prior to intravenous delivery of AAV8-SauCas9-sgRNA resulted in  
340 accumulation of cytotoxic T-cells in the liver and subsequent removal of edited hepatocytes<sup>12</sup>.  
341 Therefore, the host immune response to Cas9-AAV in mice with pre-existing immunity would likely  
342 look different than what we observed in naïve mice. In the Cas9-RNP group, we found that pre-  
343 exposing mice to SpyCas9 protein with AddaVax™ adjuvant 4 weeks prior to stereotaxic surgery  
344 synergistically increased systemic adaptive immune responses but did not result in any  
345 deleterious phenotypes in our small cohort. Further studies are needed to assess the immune  
346 response to Cas9-AAV and RNP in models with pre-existing immunity, but how well these  
347 immunized mouse models recapitulate pre-existing immunity in humans is not clear. Furthermore,  
348 breakdown of the BBB in the context of neurodegenerative disease or strong expression of the  
349 tdTomato fluorescent reporter could also impact the host immune response<sup>47,48</sup>.

350 In this study, we used a strong CMV-promoter to drive expression of SauCas9 from the  
351 AAV, which allowed us to assess all subsets of edited cells in the striatum. Although the SauCas9  
352 transgene was still expressed 4-months post-delivery, editing at predicted off-target sites was not  
353 detected. Further work to experimentally determine guide-specific off-target sites, such as Guide-

354 Seq<sup>49</sup> or Circle-Seq<sup>50</sup>, was not performed. To prevent potential genotoxic side-effects due to long-  
355 term Cas9 expression, we recommend applying additional safeguards, such as AAV self-  
356 inactivation strategies and cell-specific promoters<sup>51–53</sup>. While self-inactivating AAVs may improve  
357 safety, they may not be sufficient to reduce partial integration of the viral genome at the Cas9 cut  
358 site, which has been reported<sup>36–39</sup>. Strategies to mitigate the host response to genome editors  
359 include providing immunosuppressants with CRISPR-Cas9 infusion and screening for pre-  
360 existing immunity prior to dosing when translating *in vivo* editing to humans<sup>54</sup>.

361 In conclusion, the cell penetrant 4x-Cas9-2x NLS fusion protein enables simple and  
362 effective delivery of Cas9 RNPs into neurons *in vitro* and *in vivo*. Our study is the first to  
363 comprehensively profile the host immune response to Cas9 in the brain, benchmark an RNP  
364 delivery strategy against the gold-standard for gene delivery in the CNS, and demonstrate  
365 feasibility of large-scale manufacturing. Given that Cas9-RNPs excel at editing high levels of  
366 neurons within a localized region of the brain, this is a promising modality to characterize  
367 therapeutic benefit in disease models in the future.

## 368 **Materials & Methods**

369

### 370 *Plasmid construction*

371 Cloning of several spacers into a plasmid encoding *SauCas9* was performed as previously  
372 described. Oligonucleotides encoding sgRNAs were custom synthesized (Integrated DNA  
373 Technologies; IDT, Coralville, IA) and phosphorylated by T4 polynucleotide kinase (New England  
374 Biolabs; NEB, Ipswich, MA) for 30 min at 37°C. Oligonucleotides were annealed for 5 min at 95°C,  
375 cooled to room temperature and ligated into the *BsmBI* restriction sites of  
376 pSTX8,pKLT7.1\_SaCas9prot\_SaCas9guide plasmid. The following 23nt spacer sequences were  
377 cloned into the plasmid (spo 1: TGGTATGGCTGATTATGATCCTC; spo2:  
378 TCCCCCTGAACCTGAAACATAAA; spo3: GATGAGTTTGGACAAACCACAAC; spo4:  
379 TCCAGACATGATAAGATACATTG; spo5: CTCATCAATGTATCTTATCATGT), and plasmids  
380 were used for editing in mouse neural precursor cells *in vitro*. The best performing *SauCas9*  
381 spacer (spo4: TCCAGACATGATAAGATACATTG) was then cloned into an AAV2 backbone  
382 plasmid. pX601-AAV-CMV::NLS-SaCas9-NLS-3xHA-bGHpA;U6::BsaI-sgRNA was a gift from  
383 Feng Zhang (Addgene plasmid # 61591 ; <http://n2t.net/addgene:61591> ; RRID:Addgene\_61591).  
384 Briefly, the plasmid was digested using *BbsI* and a pair of annealed oligos were cloned into the  
385 guide RNA destination site by Golden Gate assembly. Correct construction of all plasmids was  
386 verified by Sanger sequencing (UC Berkeley DNA Sequencing Facility).

387

### 388 *Recombinant adeno-associated virus (AAV) Production*

389 The custom AAV9-CMV-61591-HA-Bgh vectors were produced at Virovek (Hayward, CA)  
390 in insect Sf9 cells by dual infection with rBV-inCap9-inRep-hr2 and rBV-CMV-61591-HA-Bgh. The  
391 AAV9-CMV-GFP vectors were produced by dual infection with rBVinCap9-inRep-hr2 and rBV-  
392 CMV-GFP. The vectors were purified through two rounds of cesium chloride (CsCl)  
393 ultracentrifugation. The CsCl was removed through buffer exchange with two PD-10 desalting

394 columns. Viral titer (approximately  $2 \times 10^{13}$  vg/mL) and purity were confirmed by nanodrop  
395 spectrophotometer, real-time PCR, and SDS-PAGE protein gel analysis. The vectors were  
396 passed through 0.2µm sterilized filters, tested for endotoxins ( $< 0.6$  EU/mL), as well as baculovirus  
397 and Sf9 DNA contamination (not detected).

398

#### 399 *Purification of low-endotoxin proteins in a laboratory setting*

400 Protein expression and purification was performed in the QB3 Macrolab at UC Berkeley  
401 using a custom low-endotoxin workflow. Briefly, the plasmid, 4xNLS-pMJ915v2 (Addgene plasmid  
402 # 88917; <http://n2t.net/addgene:88917>; RRID:Addgene\_88917), was transformed into *E. coli*  
403 Rosetta2(DE3)pLysS cells (Novagen) and an overnight culture was used to inoculate 1 L flasks  
404 (12-24 L total per batch). Cells were grown for approximately 3 hours at 37°C then cooled to  
405 16°C. At OD 0.8-0.9, cells were induced and harvested after 16-18 hours growth. Cells were lysed  
406 by homogenization in a buffer containing 1mM MgCl<sub>2</sub> and benzonase (1:1000) to help reduce  
407 viscosity and centrifuged to remove insoluble material. Purification by Ni affinity (10 mL Ni resin  
408 for every 6 L cell lysate) was performed, and the bound protein was washed with 10 column  
409 volumes of buffer containing 0.1% Triton-X114 at 4°C to help reduce endotoxins. Tag removal  
410 with TEV protease (1:100) was performed overnight at 4°C, then heparin affinity was used to  
411 concentrate each batch of protein which was then flash frozen and stored at -80°C. A Sephacryl  
412 S300 size-exclusion column (SEC) and flow path were sanitized with 0.5 M NaOH overnight, then  
413 washed with up to 3 column volumes of buffer to rinse and equilibrate the system. Frozen samples  
414 were thawed, combined, and adjusted to 4.5 mL, and the S300 standard protocol was performed  
415 for size-exclusion. Samples were refrigerated overnight, and sanitation and size-exclusion were  
416 repeated the next day to further reduce endotoxin contamination. Peak fractions were pooled,  
417 concentrated to 40µM, aliquoted at 50µL, flash frozen in liquid nitrogen, and stored at -80°C in  
418 sterile, endotoxin-free Buffer 1 (25 mM NaP (pH 7.25), 300 mM NaCl, 200 mM trehalose (Sigma  
419 Aldrich #T5251, St. Louis, MO)). Final average protein yield was 1 mg per 1 L cells. Plasmids for

420 2xNLS-SauCas9-2xNLS, 3xNLS-SauCas9-2xNLS, and 4xNLS-SauCas9-2xNLS were created by  
421 deletion mutagenesis using the existing 4xNLS construct as a template. The genes were fully  
422 sequenced to confirm no additional mutations were introduced during the mutagenesis procedure.

423

#### 424 *Purification of ultra-low endotoxin proteins in an industrial setting*

425 4x-SpyCas9-2x NLS protein was manufactured according to Aldevron proprietary  
426 workflows for expression and purification of gene editing nucleases. Briefly, the gene for 4x-  
427 SpyCas9-2x NLS was synthesized (ATUM Bio, Sunnyvale, CA) and cloned into a pD881  
428 expression vector (ATUM). Expression-ready plasmid DNA was transformed into E. coli  
429 BL21(DE3) (New England Biolabs) culture in animal-free TB media. At the appropriate OD600,  
430 expression was induced with 2.0% (w/v) Rhamnose and growth culture was harvested by  
431 centrifugation. Cells were lysed via dual-pass high-pressure homogenization and clarified via  
432 centrifugation. The clarified lysate was purified via multi-step chromatography using  
433 standard/commercially available resins. In the final chromatography step, the product is eluted  
434 via step elution and pooled to maximize final protein purity and minimize endotoxin. Product was  
435 dialyzed into the final formulation buffer, underwent three (3) exchanges of buffer, and was pooled  
436 into a sterile vessel for final filtration and dispensing. Product was evaluated for key quality  
437 attributes including endotoxin via PTS Endosafe assay (Charles River Labs, Cambridge, MA).

438

#### 439 *Quantification of endotoxins in Cas9 RNPs*

440 Proteins, guide RNAs, and pre-formed RNP complexes were subjected to several assays  
441 to quantify endotoxin burden according to the manufacturer's instructions. All assays were  
442 performed with autoclaved or certified pyrogen-free plasticware and endotoxin (ET)-free water.  
443 The plate-reader based LAL assay was performed with the Endosafe Endochrome-K kit (Charles  
444 River, #R1708K), where a control standard endotoxin (CSE) was diluted from 5 EU/mL to 0.005  
445 EU/mL. Samples were diluted 1:100 and plated in triplicate. An equal volume of LAL was added



446 to each well. A Tecan Spark plate reader (Tecan, #30086376, Männendorf, Switzerland) with  
447 SparkControl magellan V 2.2 software was used at 37°C to read absorbance at 405nm every 30  
448 seconds for 100 cycles. Time at which absorbance crossed optical density (OD) of 0.1 was  
449 recorded and used to determine endotoxin levels.

450 The cartridge-based LAL assay was performed using an Endosafe nexgen-PTS machine with  
451 R&D cartridges as recommended (Charles River, cat # PTS2005, 0.05 EU/mL sensitivity). Briefly,  
452 samples were diluted 1:50 in a large volume of ET-free water, vortexed, and 25µL was loaded  
453 into each of the four lanes of the cartridge, where two lanes contain CSE spike-in to calculate  
454 efficiency of the assay, which is valid from 50%-200% recovery. The final valid ET value was  
455 recorded from the duplicate measurement from a single cartridge.

456 The PyroGene Recombinant Factor C Endpoint Fluorescent Assay (Lonza, Walkersville, MD,  
457 cat # 50-658U) was performed as recommended. Kit-supplied CSE was diluted from 5 EU/mL to  
458 0.005 EU/mL and samples were diluted 1:100 in ET-free water and added to a plate in triplicate.  
459 The plate was heated at 37°C for 10 minutes, then an equal volume of working reagent was added  
460 to each well. Fluorescence was read immediately at time 0 and again after incubating for 60  
461 minutes. Relative fluorescence units (RFUs) of the ET-free water only blank wells were subtracted  
462 from all measurements, then delta RFUs between the two time points was calculated, and a linear  
463 regression was applied to the standard curve to calculate EUs in the samples. Fluorescence  
464 measurements were performed on a Cytation5 with Gen 5 3.04 software (BioTek, Winooski, VT).

465 HEK-Blue cells (hTLR4 and Null2) were purchased from Invivogen (San Diego, CA) and were  
466 grown under BSL2 conditions (37°C with 5% CO<sub>2</sub>) to measure SEAP production downstream of  
467 NFkappaB activation following treatment with Cas9 proteins, guide RNAs, and RNPs *in vitro* as  
468 recommended. Cells were grown in T-75 flasks with supplied antibiotic selection markers and  
469 passaged at 70% confluency. Cells were detached with gentle scraping in 1x PBS, centrifuged,  
470 counted, and plated for experiments in freshly prepared HEK-Blue Detection Media at  
471 approximately 32,000 cells per well in a 96-well plate. 180µL of cell suspension was plated directly



472 into 20 $\mu$ L of diluted CSE (5 to 0.078 ng) or samples (diluted to 10 $\mu$ M) and incubated overnight at  
473 37°C. Absorbance was read at 620nm in a Tecan Spark plate reader (Tecan, #30086376,  
474 Männendorf, Switzerland).

475

#### 476 *Neural progenitor cell (NPC) line creation and culture*

477 Neural progenitor cells were isolated from Ai9-tdTomato homozygous mouse embryos  
478 (day 13.5) by microdissection of cortical tissues into Hibernate E (#HECA, Brain Bits, LLC,  
479 Springfield, IL) and processing with the Neural Dissociation Kit with papain (#130-092-628,  
480 Miltenyi, Bergisch Gladbach, Germany) according to the manufacturer's instruction. Single cells  
481 grew into non-adherent neurospheres, which were maintained in culture media (DMEM/F12  
482 (ThermoFisher #10565-018, Waltham, MA), B-27 supplement (#12587-010), N-2 supplement  
483 (#17502-048), MEM non-essential amino acids (#11140-050), 10 mM HEPES (#15630-080),  
484 1000X 2-mercaptoethanol (#21985-023), 100X Pen/Strep (#15140-122)) supplemented with  
485 growth factors (FGF-basic (Biolegend #579606) and EGF (ThermoFisher #PHG0311) to a final  
486 concentration of 20 ng/mL in media. Neurospheres were passaged every six days using the  
487 Neural Dissociation Kit to approximately 1.5 million cells per 10-cm dish and growth factors were  
488 refreshed every 3 days. Cells were authenticated by immunofluorescent staining for Nestin and  
489 GFAP, routinely tested for mycoplasma, and were used for experiments between passages 2 and  
490 20. Dissociated cells were grown in monolayers in 96-well plates pre-coated with poly-DL-  
491 ornithine (SigmaAldrich, #P8638), laminin (SigmaAldrich #11243217001) and fibronectin  
492 (SigmaAldrich #F4759) at 10,000-30,000 cells per well for direct delivery and nucleofection  
493 experiments.

494

#### 495 *Human induced pluripotent stem cell differentiation into NPCs and culture*

496 MSC-iPSC1 cells were a generous gift from Boston Children's Hospital. iPSCs were  
497 differentiated into NPCs based on dual SMAD inhibition as previously described. Briefly, iPSCs

498 were plated onto Matrigel in the presence of 10 $\mu$ M Y-27632 (Sigma #Y0503) at a density of  
499 200,000 cells/cm<sup>2</sup>. The next day (day 0) media was changed to KSR media (Knockout DMEM  
500 (ThermoFisher #10829018), 15% Knockout serum replacement (ThermoFisher #10828010), L-  
501 glutamine (1mM), 1% MEM Non-essential amino acids, and 0.1mM B-mercaptoethanol). Media  
502 was changed daily during differentiation and gradually changed from KSR media to N2/B27 media  
503 (Neurobasal medium (ThermoFisher #21103049), GlutaMAX Supplement (ThermoFisher  
504 #35050061), N-2 supplement (ThermoFisher #17502048) and B-27 supplement (ThermoFisher  
505 #17504044)) by increasing N2/B27 media to 1/3 on day 4, 2/3 on day 6 and full N2/B27 media on  
506 day 8. For the first 12 days of differentiation media was supplemented with 100nM LDN193189  
507 (Sigma #SML0559) and 10 $\mu$ M SB431542 (Tocris Bioscience #1614, Bristol, England). For the  
508 first 4 days media was also supplemented with 2 $\mu$ M XAV939 (Tocris Bioscience #3748). On day  
509 19, NPCs were dissociated with StemPro Accutase (ThermoFisher #A1110501) and replated onto  
510 Matrigel for expansion. NPCs were passaged every 6 days and maintained in NPC media  
511 (DMEM/F12, N2 supplement, B27 supplement and 20ng/ml bFGF (Corning, #354060, Corning,  
512 NY)) with media changes every other day. For direct delivery experiments, 12,000 cells were  
513 seeded in Matrigel in a 96-well plate and treated in triplicate with 100pmol of 4xNLS-SpyCas9-  
514 2xNLS RNPs with the EMX1 guide RNA (spacer: 5' GAGTCCGAGCAGAAGAAGAA) or non-  
515 targeting guide RNA (spacer: 5' AACGACTAGTTAGGCGTGTA). In the Lipofectamine™  
516 CRISPRmax group (ThermoFisher, #CMAX00003), 3 $\mu$ g of 0xNLS-SpyCas9-2xNLS protein (18  
517 pmol) was mixed with sgRNA (1:1 molar ratio) in 8 $\mu$ L OptiMEM with 6 $\mu$ L of Cas9 Plus Reagent  
518 (1  $\mu$ g protein: 2 $\mu$ L reagent) and was mixed with a second tube containing 3.6 $\mu$ L CRISPRmax  
519 reagent in 8 $\mu$ L OptiMEM, incubated for at least 5 minutes and was immediately distributed to cells  
520 in triplicate (1 $\mu$ g RNP per well), according to the manufacturer's recommendations.

521

522 *Cas9 ribonucleoprotein (RNP) assembly and delivery to cells*

523 For cell culture experiments, RNPs were prepared immediately before use at a 1.2:1 molar  
524 ratio of single guide RNA (Synthego, Redwood City, CA) to protein (QB3 Macrolab or Aldevron).  
525 The solution was incubated for 5-10 minutes at room temperature. For nucleofection, RNPs were  
526 formed at 10 $\mu$ M in 10 $\mu$ L of pre-supplemented buffer (Lonza P3 Primary Cell 96-well Kit, #V4SP-  
527 3096). A 15 $\mu$ L suspension of 250,000 mouse NPCs was mixed with 10 $\mu$ L RNP solution and added  
528 to the nucleofection cuvette. Nucleofection was performed using the 4D Nucleofector X Unit  
529 (Lonza, #AAF-1003X) with pulse code EH-100 and cells were recovered with 75  $\mu$ L media per  
530 well approximately 2 minutes post-nucleofection. Nucleofected cells were then transferred to 100  
531  $\mu$ L fresh media in 96-well plates in triplicate and allowed to grow for 5 days at 37°C before analysis  
532 by flow cytometry for tdTomato expression. For direct delivery, RNPs were formed at 10 $\mu$ M in  
533 10 $\mu$ L of sterile Buffer 1 (25 mM sodium phosphate pH (7.25), 100 mM NaCl, 200 mM trehalose).  
534 After NPCs were grown for two days in an adherent monolayer, 10 $\mu$ L was added to cell monolayer  
535 (“direct delivery”) for a final concentration of 1 $\mu$ M (100pmol RNP/100 $\mu$ L media). Media was  
536 changed 48-hours post-treatment and cells were collected 5 days post-treatment for analysis by  
537 flow cytometry for tdTomato expression or 4 days post-treatment for DNA sequencing. For *in vivo*  
538 experiments, RNPs were prepared similarly at 10 $\mu$ M concentration in Buffer 1 and were incubated  
539 at 37°C for 10 minutes. RNPs were sterile filtered by centrifuging through 0.22 $\mu$ m Spin-X cellulose  
540 acetate membranes (Corning CoStar, #32119210) at 15,000xg for 1 minute at 4°C. RNPs were  
541 then concentrated using 100kDa Ultra-0.5 ml Centrifugal Filter Unit (Amicon, #, Burlington, MA)  
542 at 14,000xg at 4°C until the final desired concentration was reached (25-100 $\mu$ M, minimum 50 $\mu$ L  
543 volume) and collected by centrifuging at 1,000xg for 2 minutes. RNPs were then divided into  
544 single-use 20 $\mu$ L aliquots, flash frozen in liquid nitrogen, and stored at -80°C until the experiment.  
545 Prior to intracranial injection, RNPs were thawed, pipetted to mix, loaded into a 25 $\mu$ L syringe  
546 (Hamilton, #7654-01, Reno, NV) and injected with custom 29-gauge CED cannulas.

547

548 *AAV9 transduction*

549 A single 50 $\mu$ L aliquot of AAV9-CMV-SauCas9-U6-sgRNA or AAV9-CMV-GFP (Virovek)  
550 was thawed from -80°C and stored at 4°C. AAV9 was diluted in 1x PBS without calcium or  
551 magnesium to the desired concentration. For *in vivo* experiments, AAV was diluted on the day of  
552 surgeries to 3e9 vg/ $\mu$ L and stored on ice until loaded into the syringe. 5 $\mu$ L was injected in each  
553 hemisphere to a final dose of 1.5e10 vg per hemisphere using the CED. For cell culture  
554 experiments, serial dilutions were performed from 1.6e9 vg/ $\mu$ L to 2e8 vg/ $\mu$ L (lowest MOI =  
555 200,000) and 10 $\mu$ L of each were added into 96-well plates in triplicate and maintained for 3 days  
556 or 9 days prior to flow cytometry for GFP expression (transduction) and tdTomato expression  
557 (genome editing). AAV9 was added at the same time as NPC seeding for optimal transduction.

558

#### 559 *Empty capsid quantification by cryo-electron microscopy*

560 AAV samples were frozen using FEI Vitrobot Mark IV cooled down to 8°C at 100%  
561 humidity. Briefly, 4  $\mu$ L of AAV9 capsids containing GFP or Cas9 cargo was deposited on 2/2 400  
562 mesh C-flat grids (Electron Microscopy Sciences, Hatfield, PA, #CF224C-50), which were  
563 previously glow discharged at 15 mA for 15 s on PELCO easyGLOW instrument. Grids were  
564 blotted for 3 s with blot force 8 and wait time 2.5 s. Micrographs were collected manually on Talos  
565 Arctica operated at 200 kV and magnification 36,000x (pixel size 1.14 Å/pix) using a super-  
566 resolution camera setting (0.57 Å/pix) on K3 Direct Electron Detector. Micrographs were collected  
567 using SerialEM v. 3.8.7 software. Capsids were counted manually by three blinded reviewers for  
568 each image and the three counts were averaged and reported as percentage empty capsids  
569 between the two groups.

570

#### 571 *Analysis of editing in vitro*

572 tdTomato positivity was assessed by flow cytometry using IGI facilities on the Attune NxT  
573 (Thermo Fisher, AFC2). Briefly, mouse NPCs were washed once with 1x PBS, harvested with

574 0.25% trypsin, neutralized with DMEM containing 10% FBS, and resuspended in 150uL of 1x  
575 PBS per well of a round-bottom 96-well plate for analysis. The percentage of tdTomato<sup>+</sup> cells from  
576 each well was recorded. For analysis of genomic DNA (gDNA), media was removed, cells were  
577 rinsed once with 1X PBS, then incubated with 100  $\mu$ L QuickExtract solution (Lucigen  
578 Corporation Supplier Diversity Partner QuickExtract DNA Extraction Solution 1.0, Fisher,  
579 #QE09050) at 37°C for 5 minutes. The cell lysate was then moved to a thermal cycler and  
580 incubated at 65°C for 20 minutes and 95°C for 20 minutes. gDNA was used in PCR reactions to  
581 generate amplicons of approximately 150-300bp for Illumina sequencing. A list of primers used  
582 for NGS is provided in Supplementary Table 1. Sequencing was performed with Illumina MiSeq  
583 in the IGI Center for Translational Genomics and reads were analyzed in CRISPResso (website).  
584

#### 585 *Stereotaxic infusion of Cas9 RNPs and AAVs*

586 Ai9 mice (Jackson Laboratory, #007909, Bar Harbor, ME) were group housed at the  
587 University of California, Berkeley with a 12-hour light-dark cycle and allowed to feed and drink *ad*  
588 *libitum*. Housing, maintenance, and experimentation of the mice were carried out with strict  
589 adherence to ethical regulations set forth by the Animal Care and Use Committee (ACUC) at the  
590 University of California, Berkeley. Cas9-RNP and AAVs were prepared on-site at the University  
591 of California, Berkeley for injection into male and female tdTomato Ai9 mice between 2 to 5  
592 months of age. All tools were autoclaved and injected materials were sterile. Mice anesthetized  
593 with 2% isoflurane, given pre-emptive analgesics, and were arranged on Angle-two stereotactic  
594 frame (Leica, Nussloch, Germany). The incision area was swabbed with three alternating wipes  
595 of 70% ethanol and betadine scrub with sterile applicators prior to performing minimally damaging  
596 craniotomies. The stereotaxic surgery coordinates used for targeting the striatum, relative to  
597 bregma, were +0.74 mm anteroposterior,  $\pm$ 1.90 mm mediolateral, -3.37 mm dorsoventral.  
598 Bilateral infusion of Cas9 RNPs (5 $\mu$ L at 10 $\mu$ M to 100 $\mu$ M) or Cas9 AAVs (5 $\mu$ L at 3e9 vg/ $\mu$ L) was  
599 performed with a syringe pump to deliver 0.5  $\mu$ L per minute (Model 310 Plus, KD Scientific,

600 Holliston, MA). For intracerebroventricular (ICV) infusion of Cas9 RNPs, cannulas were placed at  
601  $-0.7$  mm posterior,  $\pm 1.2$  mm lateral, and  $-2.5$  mm according to Paxinos atlas of the adult mouse.  
602 Post-infusion, the syringes were left in position for 2 minutes before slow removal from the  
603 injection site, which was then cleaned, sutured, and surgically glued. Throughout the procedure,  
604 mice were kept at  $37^{\circ}\text{C}$  for warmth and Puralube Vet Ointment (Dechra, NDC #17033-211-38,  
605 Northwich, England) was applied to the outside of the eyes. For ICV injection of p0 neonatal mice,  
606 anesthesia was induced by hypothermia then  $4\mu\text{L}$  of  $100\mu\text{M}$  Cas9-RNP was injected with a hand-  
607 held 33-gauge needle unilaterally with 10% Fast Green dye to visualize distribution from one  
608 ventricle throughout the CNS. The needle was inserted 2 mm deep at a location approximately  
609  $0.25$  mm lateral to the sagittal suture and  $0.50$ - $0.75$  mm rostral to the neonatal coronal suture.  
610 RNP was slowly injected, then the needle was held in place for 15 seconds, and mice were  
611 monitored until recovery. For intrathecal injection, anesthetized mice received a 5, 25, or  $50\mu\text{L}$   
612 bolus injection of Cas9 RNP at  $300\mu\text{M}$ . The 29-gauge needle was inserted at the L6-S1 vertebral  
613 junction and angled slightly rostrally for the injection. Mice were allowed to fully recover before  
614 being transferred back to their housing. Recovery weight following all procedures was monitored  
615 daily for one week and mice were housed without further disruption for various time periods until  
616 tissue collection.

617

### 618 *Tissue collection and immunostaining*

619 At the defined study endpoints (3, 21, and 90-days post-injection), mice were placed under  
620 anesthesia and tissues were perfused with 10mL of cold PBS and 5mL of 4% paraformaldehyde  
621 (PFA, Electron Microscopy Sciences, #15710, Hatfield, PA). Brains were post-fixed overnight in  
622 4% PFA at  $4^{\circ}\text{C}$ , rinsed 3x with PBS, then cryoprotected in a 10% sucrose in PBS solution for  
623 approximately 3 days. Brains were embedded in optimal cutting temperature (OCT, Thermo  
624 Fisher, #23-730-571) media, and stored at  $-80^{\circ}\text{C}$ . Brains were cut at  $20$ - $35\mu\text{m}$ -thick sections  
625 using a cryostat (Leica CM3050S) and transferred to positively charged microscope slides. For

626 immunohistochemical analysis, tissues were blocked with solution (0.3% TritonX-100, 1% bovine  
627 serum albumin (SigmaAldrich #A9418), 5% normal goat serum (SigmaAldrich, #G9023)) before  
628 4°C incubation overnight with primary antibody in blocking solution. The next day, tissues were  
629 washed three times with PBS and incubated with secondary antibodies for one hour at room  
630 temperature. After three PBS washes, samples were incubated with DAPI solution (0.5 ug/mL,  
631 Roche LifeScience, Penzberg, Germany) as a DNA fluorescence probe for 10 minutes, washed  
632 three times with PBS, submerged once in deionized water, and mounted with glass coverslips in  
633 Fluoromount-G slide mounting medium (SouthernBiotech, Birmingham, AL). Primary antibodies  
634 included rabbit polyclonal anti-S100 $\beta$  (1:500, Abcam, #ab41548, Cambridge, England), rabbit  
635 polyclonal anti-Olig-2 (1:250, Millipore Sigma, #AB9610, Burlington, MA), rabbit polyclonal anti-  
636 doublecortin (1:800, Cell Signaling Technology, #4604, Danvers, MA), rabbit polyclonal anti-Ki67  
637 (1:100, Abcam, #ab15580), mouse monoclonal anti-NeuN (1:500, Millipore Sigma, #MAB377),  
638 rabbit polyclonal anti-DARPP-32 (1:100, Cell Signaling Technology, #2302), rabbit polyclonal  
639 anti-Iba1 (1:100, Wako Chemicals, #019-19741, Richmond, VA), mouse monoclonal anti-glia1  
640 fibrillary acidic protein (1:1000, Millipore Sigma, #MAB3402), rat monoclonal anti-CD45 (1:200,  
641 Thermo Fisher, #RA3-6B2), and rabbit polyclonal anti-CD3 (1:150, Abcam, #ab5690). Secondary  
642 antibodies included donkey anti-rat 488 (1:500, Thermo Fisher, #A-21208), goat anti-rabbit 488  
643 (1:500, Thermo Fisher, #A32731), goat anti-rabbit 647 (1:500, Thermo Fisher, #A21245), and  
644 goat anti-mouse IgG1 647 (1:500, Thermo Fisher, #A-21240).

645

#### 646 *Fluorescent imaging and image quantification*

647 Whole brain sections were imaged and stitched using the automated AxioScanZ1 (Zeiss,  
648 Oberkochen, Germany) with a 20x objective in the DAPI and tdTomato channels. Images  
649 generated from slide scanning were viewed in ZenLite software as CZI files. Images were then  
650 exported to ImageJ, Imaris, or QuPath for further quantification. The area of reflux from CED and  
651 blunt needles was calculated directly in ZenLite using the shape and area analysis tools.



652 Immunostained cells and tissues were imaged on the Evos Revolve widefield microscope using  
653 a 20x objective or Stellaris 5 confocal microscope (Leica) with a 10x or 25x water-immersion  
654 objective to capture data in DAPI, FITC, tdTomato and CY5 channels. Approximately four images  
655 were taken at 20-25x per hemisphere across multiple sections for image quantification of CD45,  
656 Iba1, and CD3 (8-12 images quantified and averaged per injection). Approximately four to six z-  
657 stack images were captured and stitched per hemisphere for qualitative images of Iba1 and for  
658 quantification of NeuN, DARPP-32, ALDH1L1, and OLIG2 with tdTomato at 1024x1024 pixel  
659 resolution with a scanning speed of 100-200.

660         Measurements of striatal editing by volume were conducted using QuPath software  
661 (version 0.3.2) from images obtained from the Zeiss AxioscanZ1. Briefly, regions of interest  
662 (ROIs) were drawn to outline the border of each striatum and the inner area of tdTomato editing  
663 using the polygon tool to create annotations. All coronal plane areas were automatically  
664 calculated. Dorsoventral coordinates (relative to bregma) were then estimated in millimeters by  
665 consulting the Mouse Brain Atlas (C57BL/6J Coronal). Approximate tissue volume was calculated  
666 by averaging outlined areas between consecutive sections to represent the mean area across a  
667 dorsoventral segment and multiplying by the difference in dorsoventral coordinates. Edited striatal  
668 volumes were then divided by total striatal volumes to obtain percent editing. Additional tdTomato<sup>+</sup>  
669 cell count measurements were conducted in Imaris software version 10.0 (Oxford Instruments,  
670 Abingdon, UK). Briefly, ROIs were drawn over each hemisphere (including cells in all brain sub-  
671 structures) using the “Segment only a Region of Interest” tool, and positive cells detected using  
672 the automated “Spots” tool to provide cell counts. Positivity thresholds were adjusted for each  
673 image to accurately capture edited cells manually. Counts of tdTomato cells on each image were  
674 then related back to approximate coordinates relative to bregma using the Mouse Brain Atlas  
675 (C57BL/6J Coronal) to quantify the distribution of edited cells.

676         Cell type specific measurements were conducted using QuPath software (version 0.3.2)  
677 on images obtained from Stellaris 5 z-stack maximal projections. ROIs were again drawn around



678 areas of observed tdTomato editing, using the polygon tool to create a single annotation per  
679 image. Cell count calculations were performed using the “Cell Detection” and “Positive Cell  
680 Detection” tools, adjusting “Cell Mean” thresholds accordingly for each channel and image.  
681 Percent area and intensity measurements were performed in Fiji/ImageJ software (version  
682 2.1.0/1.53c). Images were converted to 32-bit, and thresholds were adjusted to detect the  
683 corresponding stained area. Measurements were set to include area, minimum, maximum, and  
684 mean gray value, and area fraction, as well as to limit to threshold. All image quantification was  
685 performed on 2-5 serial sections with 3-10 independent injections per group for each analysis.  
686 Cell counts, area, intensity, and volume measurements were in general averaged from serial  
687 sections and were then grouped with other biological replicates, including independent injections,  
688 to report the treatment group average with standard deviation displayed by bar graph or box and  
689 whisker plot.

690

#### 691 *Serum collection and ELISA*

692 Blood was collected from mice at the time of euthanasia, allowed to clot at room temperature  
693 for 15-30 minutes, then centrifuged for 5 minutes at 2,000xg. Sera was collected and placed  
694 immediately on dry ice then stored at -80°C. Enzyme-linked immunosorbent assays were  
695 performed using the SeraCare Protein Detector™ HRP Microwell Anti-Mouse ELISA Kit, #5110-  
696 0011 (54-62-18) according to the manufacturer’s recommendations. First, 96-well plates were  
697 coated with antigens of interest (0.5 µg protein per well for SauCas9 and SpyCas9 (4xNLS protein  
698 variants) and approximately 1e9 empty AAV capsids per well) overnight at 4°C. Wells were  
699 washed three times and blocked at room temperature for one hour. Serum samples were then  
700 incubated in wells at varying concentrations (1:50 to 1:10,000 dilution) in 1X blocking buffer for  
701 four hours at room temperature, along with monoclonal antibody controls to generate a standard  
702 curve. Standards included CRISPR/Cas9 Monoclonal Antibody 7A9 (Epigentek, #A-9000-050,  
703 Farmingdale, NY), GenCRISPR™ SaCas9 Antibody 26H10 (GenScript, #A01952, Piscataway,

704 NJ), and Anti-Adeno-associated Virus 9 Antibody clone HL2374 (Millipore Sigma, #MABF2326-  
705 25UG). Following three additional washes, the HRP secondary antibody was added at 1:500 in  
706 1x blocking buffer and incubated for one hour. Wells were then washed three more times, and  
707 peroxidase substrate solutions were added. Absorbance was recorded at a wavelength of 405nm  
708 with Cytation5 plate reader with Gen 5 3.04 software (BioTek). Serum antibody concentrations  
709 were calculated using five-parameter logistic curve (5PL) data analysis at MyAssays.com and  
710 normalized to sham controls.

711

#### 712 *Splenocyte collection and enzyme linked immunospot (ELISpot)*

713 Splens were collected at the time of euthanasia and stored in media composed of RPMI  
714 1640 (ThermoFisher, #11875-119) with 10% FBS (VWR, #89510-186, Radnor, PA) and 1% P/S  
715 (ThermoFisher, #15140-122). Briefly, spleens were physically dissociated by forcing through a  
716 100µm cell strainer in 10mL of media then single cells were passed through a 70µm strainer and  
717 centrifuged at 200xg for 5 minutes. Cells were resuspended in 5mL of 1x RBC Lysis Buffer  
718 (Miltenyi # 130-094-183) for approximately 3 minutes, then centrifuged again and resuspended in  
719 media for counting. The mouse interferon-gamma (IFN-γ) ELISpot kit (R&D Systems, #EL485,  
720 Minneapolis, MN) was used according to the manufacturer's instructions to assess activation of  
721 splenocytes, containing T-cells, in response to treatment with Cas9 proteins. Briefly, the plate was  
722 pre-washed and 200µL of media for at least 20 minutes in the incubator, prior to adding cells at  
723 300,000 per well in 100µL media. Treatments at 2x dose were prepared in media and 100µL was  
724 added to wells in triplicate (final 5 µg/mL concentration). Plates were wrapped in foil and incubated  
725 for 48 hours without disturbing. Concanavalin A (SigmaAldrich, #C5275) was used as a positive  
726 control for cell mediated IFN-γ production (final 4 µg/mL concentration). After 48-hours, cells were  
727 removed and the secreted analyte was detected with immunostaining using the kit-provided  
728 biotinylated monoclonal antibody specific for mouse IFN-γ, streptavidin-conjugated alkaline

729 phosphatase, and stabilized detection mixture of 5-Bromo-4-Chloro-3'Indolylphosphate-p-  
730 Toluidine Salt (BCIP) and Nitro Blue Tetrazolium Chloride (NBT). After staining, plates were dried  
731 overnight and spot forming units were imaged and counted on the ImmunoSpot S6 Macro  
732 Analyzer (Cellular Technology Limited, Shaker Heights, OH).

733

#### 734 *Immunization of mice to Cas9 with adjuvant*

735 AddaVax™ (Invivogen, vac-adx-10), a squalene-based oil-in-water nano-emulsion, was  
736 mixed with an equal volume containing 25µg of 4x-SpyCas9-2x protein diluted in sterile buffer at  
737 room temperature for a final injection volume of 50µL. Mice received two 25µL subcutaneous  
738 injections of the AddaVax:Cas9 mixture (immunized) or AddaVax:Buffer alone (sham) with a 30-  
739 gauge insulin syringe into each flank. After four weeks, stereotaxic surgery with bilateral injections  
740 of 5µL of 25µM Cas9-RNPs was performed in a subset of mice. Mice showed no signs of pain or  
741 distress following treatment with AddaVax and no acute events were noted after surgery. Mice  
742 that received AddaVax, with or without surgery, were euthanized 6-weeks post-subcutaneous  
743 injections. Brains, serum, and spleens were collected for analysis of adaptive immune responses  
744 against repeated exposure to Cas9.

745

#### 746 *DNA/RNA extraction from brain tissue slices and quantitative RT-PCR, droplet digital PCR, and* 747 *long-read sequencing*

748 Brains were collected at 3, 14, and 28-days or 4-months for DNA and RNA analysis.  
749 Briefly, mice were placed under anesthesia and perfused with cold PBS. Brains were harvested  
750 and cut into 2-mm sections using a matrix around the injection site (Zivic Instruments, Pittsburgh,  
751 PA). The slices were transferred onto chilled glass slides and further trimmed to approximate  
752 30mg tissue weight (1–1.25 mm wide × 2 mm long). Tissues were flash frozen in liquid nitrogen  
753 then stored at -80°C until processing. DNA and RNA were collected from tissues using the AllPrep  
754 DNA/RNA Mini Kit (Qiagen, #80204, Venlo, Netherlands) according to the manufacturer's

755 instructions. Briefly, brains were homogenized in 1.5 mL tubes with a disposable pestle directly in  
756 RLT lysis buffer supplemented with 2-mercaptoethanol, then passed through Qiashredder  
757 columns to further homogenize prior to adding directly to the DNA and RNA binding columns.  
758 DNA was eluted in 100 $\mu$ L of EB, and RNA was eluted in 40  $\mu$ L RNase-free water. Concentrations  
759 of nucleic acids were measured by nanodrop spectrophotometer and samples were stored at -  
760 20°C.

761 Gene expression was quantified across multiple samples using a Custom RT<sup>2</sup> PCR Array  
762 (Qiagen, #330171, CLAM45824) and analyzed using the RT<sup>2</sup> Profiler PCR Data Analysis Tool on  
763 GeneGlobe (Qiagen). For reverse transcription, the RT<sup>2</sup> First Strand Kit (Qiagen, #330404) was  
764 used according to the manufacturer's instructions. cDNA was diluted in water and added to the  
765 RT<sup>2</sup> SYBR Green qPCR Mastermix (Qiagen, #330502) then distributed across the 24-wells  
766 containing verified assay primers and controls (PCR array reproducibility control, reverse  
767 transcription efficiency control, genomic DNA contamination control, two house-keeping genes,  
768 and 19 experimental genes). Quantitative real-time PCR was performed on the CFX96 Touch  
769 Real-Time PCR System (BioRad). cDNA was also used in a droplet digital PCR reaction to  
770 measure SauCas9 expression at the 4-month time-point. qPCR assay IDs are included in Tables  
771 S1 and S2.

772 DNA was also used for PCR amplicon sequencing of predicted off-target sites and for  
773 droplet digital PCR (ddPCR). Off-target sites were predicted using Cas-OFFinder  
774 (<http://www.rgenome.net/cas-offinder/>)<sup>55</sup>. Predicted off-targets are described further in Tables S3  
775 and S4. Primers were designed using NCBI Primer Blast with an amplicon size of 250-300bp,  
776 listed in Table S1. Sequencing was performed with Illumina MiSeq in the IGI Center for  
777 Translational Genomics and reads were analyzed in CRISPResso2  
778 (<http://crispresso.pinellolab.org>)<sup>56</sup>.

779 For droplet digital PCR (ddPCR), a custom NHEJ ddPCR assays were generated using  
780 the online Bio-Rad design tool (Table S2). Assays for SauCas9 and SpyCas9 contain both the

781 primers and probes (HEX-probe spanning the cut-site and a distal reference FAM-probe). To  
782 prepare the reactions, 110 ng of gDNA was combined with the 20x assay, 2x ddPCR Supermix  
783 for Probes (No dUTP), 1 $\mu$ L of of Smal restriction enzyme (2 units per reaction), and water up to  
784 22 $\mu$ L. Then 20  $\mu$ l of each reaction mix was added to DG8TM Cartridges (Bio-Rad #1864008,  
785 Hercules, CA) followed by 70  $\mu$ l of Droplet Generation Oil for Probes (Bio-Rad #1863005) and  
786 droplets were formed in the QX200 Droplet Generator. Droplets were then transferred to a 96-  
787 well plate and thermal cycled according to the manufacturer's recommendation with a 3-minute  
788 annealing/extension step. After thermal cycling, the sealed plate was placed in the QX200 Droplet  
789 Reader and data was acquired and analyzed in the QuantaSoft Analysis Pro Software using the  
790 "Drop-Off" analysis, manually setting the thresholds for cluster calling (FAM+ only, FAM+ HEX+  
791 cluster, FAM-HEX- cluster), and exporting fractional abundance calculations.

792 Long-read sequencing of the tdTomato locus was performed on DNA isolated from the  
793 treated mouse brains. Briefly, PCR amplicons were generated on 16 samples from the 4-month  
794 treatment groups using primers with unique barcodes for sample de-multiplexing. The KAPA HiFi  
795 Hotstart PCR Kit (Roche, KK2502) was used to amplify the 1100 bp product and reactions were  
796 cleaned with AMPure XP magnetic beads (Beckman Coulter Inc., Brea, CA) prior to analysis by  
797 Qubit and Bioanalyzer with the DNA 7500 Kit (Agilent, #5067-1506, Santa Clara, CA). Samples  
798 were combined and 1 $\mu$ g of pooled amplicons and submitted (> 20ng/ $\mu$ L) for sequencing with one  
799 PacBio Sequel 8M SMRT Cell at the QB3 Vincent Coates Genomic Sequencing Lab, yielding  
800 approximately 110,000 reads per sample. Data were analyzed using a custom pipeline to identify  
801 viral fragment trapping during DNA repair. Briefly, PacBio circular consensus reads were trimmed  
802 with Cutadapt (Version 4.1)<sup>57</sup>, then aligned to the AAV vector using NGMLR (Version 0.2.7)<sup>58</sup> to  
803 generate BAM files. Soft-clipped regions of aligned reads were extracted using PySam (Version  
804 0.18.0, <https://github.com/pysam-developers/pysam>) to parse CIGAR strings, then realigned to  
805 the tdTomato locus with NGMLR to verify integration within 200 bp of the cut site. Confirmed

806 integrations were visualized along the AAV genome using pyGenomeTracks (Version 3.3) and  
807 coverage statistics were summarized using PySam<sup>59,60</sup>.

808

### 809 *Statistical analyses*

810 The data presented in bar graphs and box and whisker plots are averages across multiple  
811 technical and biological replicates and error bars represent the standard deviation. Sample sizes  
812 are indicated in the text and figure legends and generally refer to technical injection replicates  
813 (two technical replicates, i.e., bilateral injections, per one biological replicate). When comparing  
814 two groups with normal distribution, an unpaired student's t-test was performed in Prism 9  
815 (GraphPad Software version 9.4.1). When comparing multiple groups, a one-way ANOVA with  
816 Tukey's multiple comparison test was performed in Prism 9 (GraphPad Software version 9.4.1).  
817 The RT-qPCR experiments used Student's t-test of the experimental group compared to the sham  
818 control (Qiagen GeneGlobe RT<sup>2</sup> Profiler PCR Data Analysis).  $p \leq 0.05$  was considered significant

819

### 820 **Data Availability Statement**

821 Long-read sequencing (BAM files from PacBio circular consensus sequence, CCS) are  
822 available in Sequence Read Archive (SRA). Accession number: [#]. All additional data is  
823 available upon request.

824

### 825 **Acknowledgements**

826 Thank you to Netravathi Krishnappa and Christopher Hann-Soden for library preparation,  
827 sequencing, and analysis at the IGI Center for Translational Genomics and the QB3 Vincent J.  
828 Coates Genomics Sequencing Lab. Thank you to members of the Doudna lab at IGI, particularly  
829 Drs. Matthew Kan and Jennifer Hamilton, as well as Brett Staahl, Ross Wilson, and Fyodor Urnov  
830 for intellectual contributions and support. Thank you to Aldevron, LLC for collaboration on this

831 effort, especially Samantha Foti, Allison Pappas, David Yoder, and Max Sellman. Thank you to  
832 Denise Schichnes and Steven Ruzin at the CNR Berkeley Imaging Facility at the University of  
833 California, Berkeley as well as Feather Ives, Anita Flynn, and Holly Aaron at the CRL Microscopy  
834 Imaging Core (RRID:SCR\_017852) at the University of California, Berkeley. Thank you to Eva  
835 Harris and lab members for the use of the ELISpot plate reader. Thank you to Kathy Snow and  
836 Ethan Saville at Jackson Laboratories for discussion about QuPath image quantification software.  
837 Thank you to Drs. Greg Barton and David Raulet for intellectual discussions regarding endotoxins  
838 and immune response. Thank you to Biogen Inc., especially Robin Kleinmen and Anirvan Ghosh,  
839 for funding and intellectual contributions. Thank you to Ruth L. Kirschstein F32 NIGMS for funding  
840 (E.C.S).

841

#### 842 **Author Contributions**

843 E.C.S performed the experiments, analysis, and manuscript preparation and oversaw  
844 contributions from researchers (R.A., E. A., S.E.K., A.S., N.L., M.K.) who assisted with tissue  
845 processing, cloning, ELISAs, immunohistochemistry, and image analysis. E.C.S., J.K.S., and  
846 M.H.K. designed *in vivo* experiments, performed stereotaxic surgeries, confocal microscopy, and  
847 quantitative PCR. M.T. performed long-read NGS sequencing analysis. E.C.S. performed  
848 isolation and culture of mouse primary cells, flow cytometry, and ELISpot assays. K.S. performed  
849 electron microscopy. V.S.R. and L.T.V. performed human stem cell culture and differentiation.  
850 C.J., A.W., T.M., A.K., and T.F. performed custom low-endotoxin protein expression and  
851 purification. D.F.S. and J.A.D. approved the experiments, provided intellectual contributions, and  
852 co-wrote the manuscript.

853

#### 854 **Declaration of Interests Statement**

855 J.A.D. is a cofounder of Caribou Biosciences, Editas Medicine, Scribe Therapeutics, Intellia  
856 Therapeutics and Mammoth Biosciences. J.A.D. is a scientific advisory board member of Vertex,

857 Caribou Biosciences, Intellia Therapeutics, eFFECTOR Therapeutics, Scribe Therapeutics,  
858 Mammoth Biosciences, Synthego, Algen Biotechnologies, Felix Biosciences, The Column Group  
859 and Inari. J.A.D. is a Director at Johnson & Johnson and Tempus and has research projects  
860 sponsored by Biogen, Pfizer, Apple Tree Partners and Roche. Patent applications have been filed  
861 relating to the technologies described herein. The indicated authors are employees of Aldevron,  
862 LLC, which offers proteins, pDNA, mRNA and reagents for sale similar to some of the compounds  
863 described in this manuscript.

864

865 **Keywords (5-10)**

866 CRISPR-Cas9, Genome Editing, Viral Vectors, Non-viral Delivery, Mouse, Brain, Host Immune  
867 Response, Neurons, Microglia, Endotoxin/LPS

868

869

870



871 **References**

872

873 1. Heidenreich, M. & Zhang, F. Applications of CRISPR–Cas systems in neuroscience. *Nat Rev*  
874 *Neurosci* **17**, 36–44 (2016).

875 2. The SCGE Consortium *et al.* The NIH Somatic Cell Genome Editing program. *Nature* **592**,  
876 195–204 (2021).

877 3. Jinek, M. *et al.* A Programmable Dual-RNA–Guided DNA Endonuclease in Adaptive Bacterial  
878 Immunity. *Science* **337**, 816–821 (2012).

879 4. Jinek, M. *et al.* RNA-programmed genome editing in human cells. *eLife* **2**, e00471 (2013).

880 5. Doudna, J. A. The promise and challenge of therapeutic genome editing. *Nature* **578**, 229–  
881 236 (2020).

882 6. Hadaczek, P. *et al.* Transduction of Nonhuman Primate Brain with Adeno-Associated Virus  
883 Serotype 1: Vector Trafficking and Immune Response. *Human Gene Therapy* **20**, 225–237  
884 (2009).

885 7. Ciesielska, A. *et al.* Cerebral Infusion of AAV9 Vector-encoding Non-self Proteins Can Elicit  
886 Cell-mediated Immune Responses. *Molecular Therapy* **21**, 158–166 (2013).

887 8. Samaranch, L. *et al.* AAV9-mediated Expression of a Non-self Protein in Nonhuman Primate  
888 Central Nervous System Triggers Widespread Neuroinflammation Driven by Antigen-  
889 presenting Cell Transduction. *Molecular Therapy* **22**, 329–337 (2014).

890 9. Agustín-Pavón, C., Mielcarek, M., Garriga-Canut, M. & Isalan, M. Deimmunization for gene  
891 therapy: host matching of synthetic zinc finger constructs enables long-term mutant  
892 Huntingtin repression in mice. *Mol Neurodegeneration* **11**, 64 (2016).

- 893 10. Chew, W. L. *et al.* A multifunctional AAV–CRISPR–Cas9 and its host response. *Nat Methods*  
894 **13**, 868–874 (2016).
- 895 11. Moreno, A. M. *et al.* immune-orthogonal orthologues of AAV capsids and of Cas9  
896 circumvent the immune response to the administration of gene therapy. *Nat Biomed Eng* **3**,  
897 806–816 (2019).
- 898 12. Li, A. *et al.* AAV-CRISPR Gene Editing Is Negated by Pre-existing Immunity to Cas9.  
899 *Molecular Therapy* **28**, 1432–1441 (2020).
- 900 13. Simhadri, V. L. *et al.* Prevalence of Pre-existing Antibodies to CRISPR-Associated Nuclease  
901 Cas9 in the USA Population. *Molecular Therapy - Methods & Clinical Development* **10**, 105–  
902 112 (2018).
- 903 14. Charlesworth, C. T. *et al.* Identification of preexisting adaptive immunity to Cas9 proteins in  
904 humans. *Nat Med* **25**, 249–254 (2019).
- 905 15. Wagner, D. L. *et al.* High prevalence of *Streptococcus pyogenes* Cas9-reactive T cells within  
906 the adult human population. *Nat Med* **25**, 242–248 (2019).
- 907 16. Ferdosi, S. R. *et al.* Multifunctional CRISPR-Cas9 with engineered immunosilenced human T  
908 cell epitopes. *Nat Commun* **10**, 1842 (2019).
- 909 17. Tang, X.-Z. E., Tan, S. X., Hoon, S. & Yeo, G. W. Pre-existing adaptive immunity to the RNA-  
910 editing enzyme Cas13d in humans. *Nat Med* **28**, 1372–1376 (2022).
- 911 18. Mingozzi, F. & High, K. A. Immune responses to AAV vectors: overcoming barriers to  
912 successful gene therapy. *Blood* **122**, 23–36 (2013).
- 913 19. Staahl, B. T. *et al.* Efficient genome editing in the mouse brain by local delivery of  
914 engineered Cas9 ribonucleoprotein complexes. *Nat Biotechnol* **35**, 431–434 (2017).

- 915 20. Liu, J., Gaj, T., Wallen, M. C. & Barbas, C. F. Improved Cell-Penetrating Zinc-Finger Nuclease  
916 Proteins for Precision Genome Engineering. *Molecular Therapy - Nucleic Acids* **4**, e232  
917 (2015).
- 918 21. Madisen, L. *et al.* A robust and high-throughput Cre reporting and characterization system  
919 for the whole mouse brain. *Nat Neurosci* **13**, 133–140 (2010).
- 920 22. Oura, S. *et al.* Precise CAG repeat contraction in a Huntington’s Disease mouse model is  
921 enabled by gene editing with SpCas9-NG. *Commun Biol* **4**, 771 (2021).
- 922 23. Ran, F. A. *et al.* In vivo genome editing using Staphylococcus aureus Cas9. *Nature* **520**, 186–  
923 191 (2015).
- 924 24. Maeder, M. L. *et al.* Development of a gene-editing approach to restore vision loss in Leber  
925 congenital amaurosis type 10. *Nat Med* **25**, 229–233 (2019).
- 926 25. Yin, C. *et al.* In Vivo Excision of HIV-1 Provirus by saCas9 and Multiplex Single-Guide RNAs in  
927 Animal Models. *Molecular Therapy* **25**, 1168–1186 (2017).
- 928 26. Gao, G. *et al.* Clades of Adeno-Associated Viruses Are Widely Disseminated in Human  
929 Tissues. *J Virol* **78**, 6381–6388 (2004).
- 930 27. Smith, R. H., Levy, J. R. & Kotin, R. M. A Simplified Baculovirus-AAV Expression Vector  
931 System Coupled With One-step Affinity Purification Yields High-titer rAAV Stocks From  
932 Insect Cells. *Molecular Therapy* **17**, 1888–1896 (2009).
- 933 28. Chen, C., Akerstrom, V., Baus, J., Lan, M. S. & Breslin, M. B. Comparative analysis of the  
934 transduction efficiency of five adeno associated virus serotypes and VSV-G pseudotype  
935 lentiviral vector in lung cancer cells. *Virol J* **10**, 86 (2013).

- 936 29. Gaj, T. *et al.* Targeted gene knock-in by homology-directed genome editing using Cas9  
937 ribonucleoprotein and AAV donor delivery. *Nucleic Acids Research* **45**, e98–e98 (2017).
- 938 30. Park, I.-H. *et al.* Reprogramming of human somatic cells to pluripotency with defined  
939 factors. *Nature* **451**, 141–146 (2008).
- 940 31. Qi, Y. *et al.* Combined small-molecule inhibition accelerates the derivation of functional  
941 cortical neurons from human pluripotent stem cells. *Nat Biotechnol* **35**, 154–163 (2017).
- 942 32. Chambers, S. M. *et al.* Highly efficient neural conversion of human ES and iPS cells by dual  
943 inhibition of SMAD signaling. *Nat Biotechnol* **27**, 275–280 (2009).
- 944 33. Fu, Y. *et al.* High-frequency off-target mutagenesis induced by CRISPR-Cas nucleases in  
945 human cells. *Nat Biotechnol* **31**, 822–826 (2013).
- 946 34. Bobo, R. H. *et al.* Convection-enhanced delivery of macromolecules in the brain. *Proc. Natl.*  
947 *Acad. Sci. U.S.A.* **91**, 2076–2080 (1994).
- 948 35. Hadaczek, P. *et al.* Convection-Enhanced Delivery of Adeno-Associated Virus Type 2 (AAV2)  
949 into the Striatum and Transport of AAV2 Within Monkey Brain. *Human Gene Therapy* **17**,  
950 291–302 (2006).
- 951 36. Hanlon, K. S. *et al.* High levels of AAV vector integration into CRISPR-induced DNA breaks.  
952 *Nat Commun* **10**, 4439 (2019).
- 953 37. Nelson, C. E. *et al.* Long-term evaluation of AAV-CRISPR genome editing for Duchenne  
954 muscular dystrophy. *Nat Med* **25**, 427–432 (2019).
- 955 38. Ferrari, S. *et al.* Choice of template delivery mitigates the genotoxic risk and adverse impact  
956 of editing in human hematopoietic stem cells. *Cell Stem Cell* **29**, 1428-1444.e9 (2022).

- 957 39. Simpson, B. P., Yrigollen, C. M., Izda, A. & Davidson, B. L. Targeted long-read sequencing  
958 captures CRISPR editing and AAV integration outcomes in brain. *Molecular Therapy*  
959 S1525001623000047 (2023) doi:10.1016/j.ymthe.2023.01.004.
- 960 40. Zink McCullough, K. *Calculating Endotoxin Limits for Drug Products*.  
961 [https://www.acciusa.com/pdfs/supplements/Endotoxin%20Detection%20Part%20VI/Calcul](https://www.acciusa.com/pdfs/supplements/Endotoxin%20Detection%20Part%20VI/Calculating_Endotoxin_Limits.pdf)  
962 [ating\\_Endotoxin\\_Limits.pdf](https://www.acciusa.com/pdfs/supplements/Endotoxin%20Detection%20Part%20VI/Calculating_Endotoxin_Limits.pdf).
- 963 41. Lee, B. *et al.* Nanoparticle delivery of CRISPR into the brain rescues a mouse model of fragile  
964 X syndrome from exaggerated repetitive behaviours. *Nat Biomed Eng* **2**, 497–507 (2018).
- 965 42. Park, H. *et al.* In vivo neuronal gene editing via CRISPR–Cas9 amphiphilic nanocomplexes  
966 alleviates deficits in mouse models of Alzheimer’s disease. *Nat Neurosci* **22**, 524–528  
967 (2019).
- 968 43. Metzger, J. M. *et al.* Efficient in vivo neuronal genome editing in the mouse brain using  
969 nanocapsules containing CRISPR-Cas9 ribonucleoproteins. *Biomaterials* **293**, 121959 (2023).
- 970 44. Wang, Y. *et al.* Overcoming the Blood–Brain Barrier for Gene Therapy via Systemic  
971 Administration of GSH-Responsive Silica Nanocapsules. *Advanced Materials* 2208018 (2022)  
972 doi:10.1002/adma.202208018.
- 973 45. Yan, S. *et al.* Cas9-mediated replacement of expanded CAG repeats in a pig model of  
974 Huntington’s disease. *Nat. Biomed. Eng* (2023) doi:10.1038/s41551-023-01007-3.
- 975 46. He, M. *et al.* A traceless linker for aliphatic amines that rapidly and quantitatively fragments  
976 after reduction. *Chem. Sci.* **11**, 8973–8980 (2020).
- 977 47. Sweeney, M. D., Sagare, A. P. & Zlokovic, B. V. Blood–brain barrier breakdown in Alzheimer  
978 disease and other neurodegenerative disorders. *Nat Rev Neurol* **14**, 133–150 (2018).

- 979 48. Huang, L. *et al.* Expression of tdTomato and luciferase in a murine lung cancer alters the  
980 growth and immune microenvironment of the tumor. *PLoS ONE* **16**, e0254125 (2021).
- 981 49. Tsai, S. Q. *et al.* GUIDE-seq enables genome-wide profiling of off-target cleavage by CRISPR-  
982 Cas nucleases. *Nat Biotechnol* **33**, 187–197 (2015).
- 983 50. Tsai, S. Q. *et al.* CIRCLE-seq: a highly sensitive in vitro screen for genome-wide CRISPR–Cas9  
984 nuclease off-targets. *Nat Methods* **14**, 607–614 (2017).
- 985 51. Ibraheim, R. *et al.* Self-inactivating, all-in-one AAV vectors for precision Cas9 genome  
986 editing via homology-directed repair in vivo. *Nat Commun* **12**, 6267 (2021).
- 987 52. Li, A. *et al.* A Self-Deleting AAV-CRISPR System for In Vivo Genome Editing. *Mol Ther*  
988 *Methods Clin Dev* **12**, 111–122 (2019).
- 989 53. Merienne, N. *et al.* The Self-Inactivating KamiCas9 System for the Editing of CNS Disease  
990 Genes. *Cell Rep* **20**, 2980–2991 (2017).
- 991 54. Ewaisha, R. & Anderson, K. S. Immunogenicity of CRISPR therapeutics—Critical  
992 considerations for clinical translation. *Front. Bioeng. Biotechnol.* **11**, 1138596 (2023).
- 993 55. Bae, S., Park, J. & Kim, J.-S. Cas-OFFinder: a fast and versatile algorithm that searches for  
994 potential off-target sites of Cas9 RNA-guided endonucleases. *Bioinformatics* **30**, 1473–1475  
995 (2014).
- 996 56. Clement, K. *et al.* CRISPResso2 provides accurate and rapid genome editing sequence  
997 analysis. *Nat Biotechnol* **37**, 224–226 (2019).
- 998 57. Martin, M. Cutadapt removes adapter sequences from high-throughput sequencing reads.  
999 *EMBnet j.* **17**, 10 (2011).

- 1000 58. Sedlazeck, F. J. *et al.* Accurate detection of complex structural variations using single-  
1001 molecule sequencing. *Nat Methods* **15**, 461–468 (2018).
- 1002 59. Ramírez, F. *et al.* High-resolution TADs reveal DNA sequences underlying genome  
1003 organization in flies. *Nat Commun* **9**, 189 (2018).
- 1004 60. Lopez-Delisle, L. *et al.* pyGenomeTracks: reproducible plots for multivariate genomic  
1005 datasets. *Bioinformatics* **37**, 422–423 (2021).
- 1006
- 1007



1008 **Figure Legends**

1009

1010 **Figure 1. In vivo editing at tdTomato locus with viral and non-viral Cas9 delivery**

1011 **strategies.** (A) Schematic of 4x-SpyCas9-2x cell-penetrating protein expression and purification  
1012 systems, (B) AAV9-SauCas9-sgRNA expression and purification systems, (C) and expected  
1013 edited brain regions in the partial basal ganglia direct circuit shown in sagittal view (top) and  
1014 coronal view (bottom). Neurons extend from the striatum into the globus pallidus (GP) and  
1015 substantia nigra (SNr). Created with BioRender.com. (D) Comparison of standard blunt ended  
1016 needles versus those fitted with CED cannula had a similar amount of edited striatal volume and  
1017 markers of tissue damage (supplement), however the CED needle significantly reduced reflux of  
1018 RNP back up the needle injection track (n=3-6 injections per group, \*\* p<0.01.) Scale bar:1 mm.  
1019 (E) Serial sections of single hemisphere sagittal view of edited tdTomato+ cells in the basal  
1020 ganglia circuit after injection of Cas9 RNP with CED into the striatum, with signal detected near  
1021 the GP and SNr. Scale bar: 1 mm. (F) Representative coronal section of the striatum of mice  
1022 that received Cas9 RNPs and AAVs at 21 days post-injection, showing the distribution of  
1023 tdTomato+ edited cells. Scale bar: 1 mm. (G) Co-staining of tdTomato with NeuN and GFAP  
1024 showed that neurons were the predominately edited cell type in the striatum (>99% of  
1025 tdTomato+ cells in the edited region of interest co-expressed NeuN in Cas9 AAV and Cas9  
1026 RNP at 125pmol). However, at doses of Cas9 RNPs greater than 125pmol, a decrease in NeuN  
1027 staining and an increase in GFAP staining was observed out to 90-days. Scale bar: 50  $\mu$ m. (H)  
1028 The volume of edited striatal tissue was stable as the concentration of injected Cas9 RNPs was  
1029 increased from 10 to 100  $\mu$ M (n=4-6 injections). Since 125pmol dose had the highest maximal  
1030 level of detected editing, we proceeded with this dose for subsequent studies. (I) Cas9 AAV had  
1031 significantly greater edited striatal tissue than Cas9 RNPs at 125pmol dose at 21 and 90-days  
1032 post-injection (n=4-6 injections, \* p< 0.05). (J) Within the region of interest (ROI) Cas9 RNPs

1033 edited approximately 36% of NeuN+ neurons, while Cas9 AAV edited approximately 20% of  
1034 neurons. Scale bar: 250  $\mu\text{m}$ .

1035

1036 **Figure 2. Immune response to in vivo editing with viral and non-viral Cas9 delivery**

1037 **strategies.** (A) Representative immunostaining of Iba1 (microglia, green) with tdTomato and

1038 DAPI using confocal microscopy. Scale bar: 50  $\mu\text{m}$ . (B) Quantification of Iba1<sup>+</sup> cells, staining

1039 intensity, and percent area (n=4-6 technical replicates, one-way ANOVA, \*p<0.05). (C)

1040 Quantification of CD45<sup>+</sup> and CD3<sup>+</sup> cells per image (n=3-6 replicates, one-way ANOVA, ns) with

1041 representative confocal images. (D) Representative images of CD45, CD3, and Iba1 showing

1042 co-expression of CD45 (green) with both Iba1 (microglia, red) and CD3 (T-cells, red) cells and

1043 differential cell morphology. Merged images include DAPI (gray) and tdTomato (magenta).

1044 Scale bar: 50  $\mu\text{m}$ . (E) Quantification of IgG antibodies against Cas9 or AAV capsid proteins

1045 measured 28 and 90-days after bilateral intrastriatal injections by ELISA (n=3-5 biological

1046 replicates). (F) Heat map summarizing RT-qPCR results of 21 genes at two time-points. At each

1047 time point, Ppih was used as a housekeeping control for delta-delta Ct analysis and compared

1048 to the sham group using Qiagen analysis portal (n=4, \*p < 0.05).

1049

1050 **Figure 3. Optimized, low-endotoxin RNP formulation reduces local immune response.** (A)

1051 Schematic of manufacturing scale up to produce industrial quantity of ultra-low endotoxin 4x-

1052 SpyCas9-2x protein using a tag-free expression and purification system. (B) Endotoxin levels

1053 calculated on a per mouse basis between the standard (laboratory 4x-SpyCas9-2x with sg298

1054 2018) and optimized (industrial 4x-SpyCas9-2x protein with sg298 2022) RNP formulations at

1055 25 $\mu\text{M}$  measured by LAL assay. The optimized RNP had a final endotoxin level of 0.44 EU/kg,

1056 just above the FDA recommendation of 0.2 EU/kg/hr (dotted line) for human drug products

1057 administered into the central nervous system. (C) Quantification of Iba1<sup>+</sup> staining intensity and

1058 percent area (n=6-10, one-way ANOVA, \*p<0.05). (D) Quantification of CD45<sup>+</sup> and (E) CD3<sup>+</sup>  
1059 cells per image (n=6-10, one-way ANOVA, ns). (F) Percent volume of edited striatal tissue for  
1060 Cas9 RNPs injected at 25μM (n=6-10 injections). (G) Quantification of IgG antibodies against  
1061 Cas9 or AAV capsid proteins measured 21-days after bilateral intrastriatal injections by ELISA  
1062 (n=3-5 biological replicates).  
1063

Figure 1. In vivo editing at tdTomato locus with viral and non-viral Cas9 delivery strategies

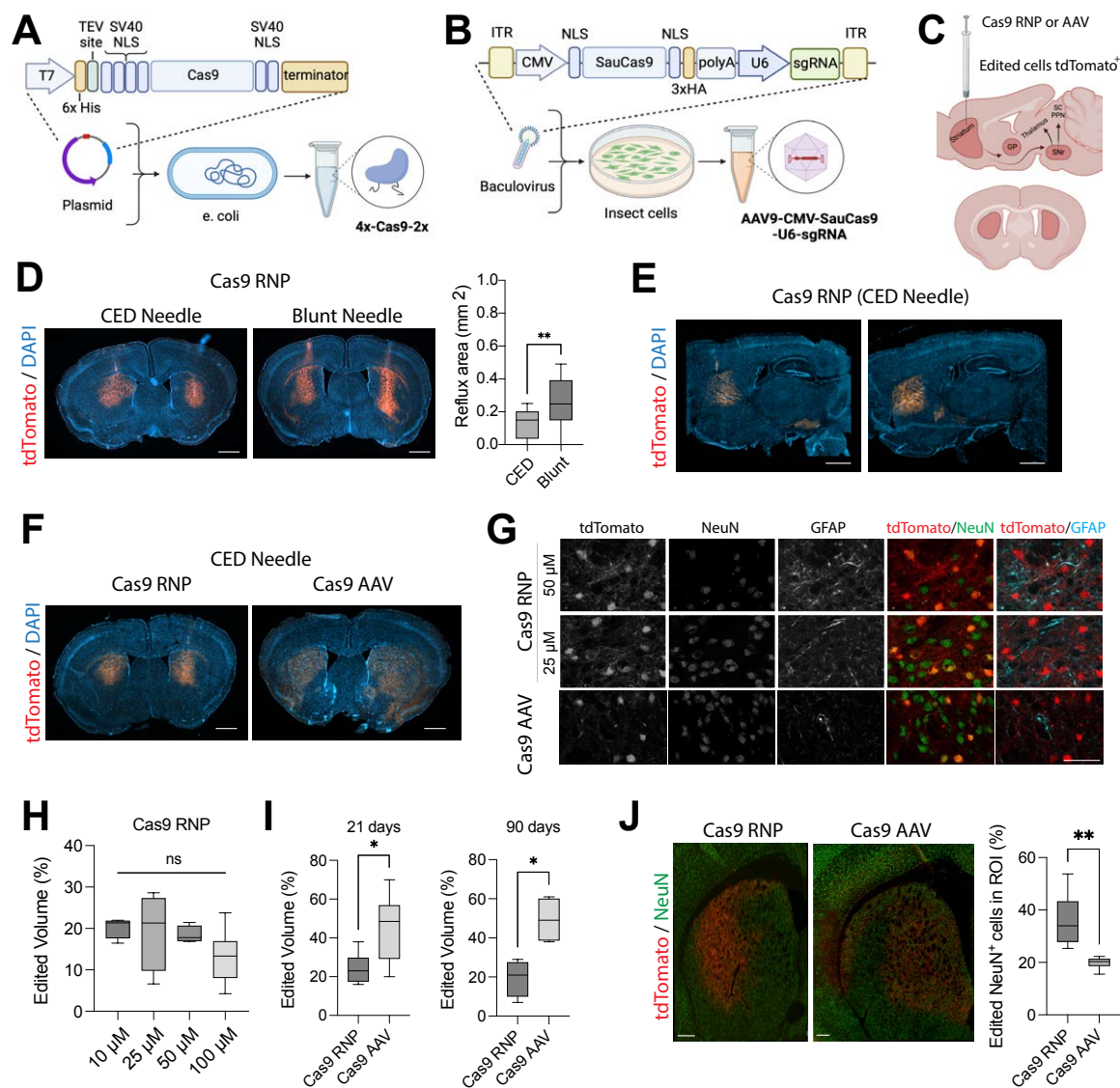


Figure 2. Immune response to in vivo editing with viral and non-viral Cas9 delivery strategies

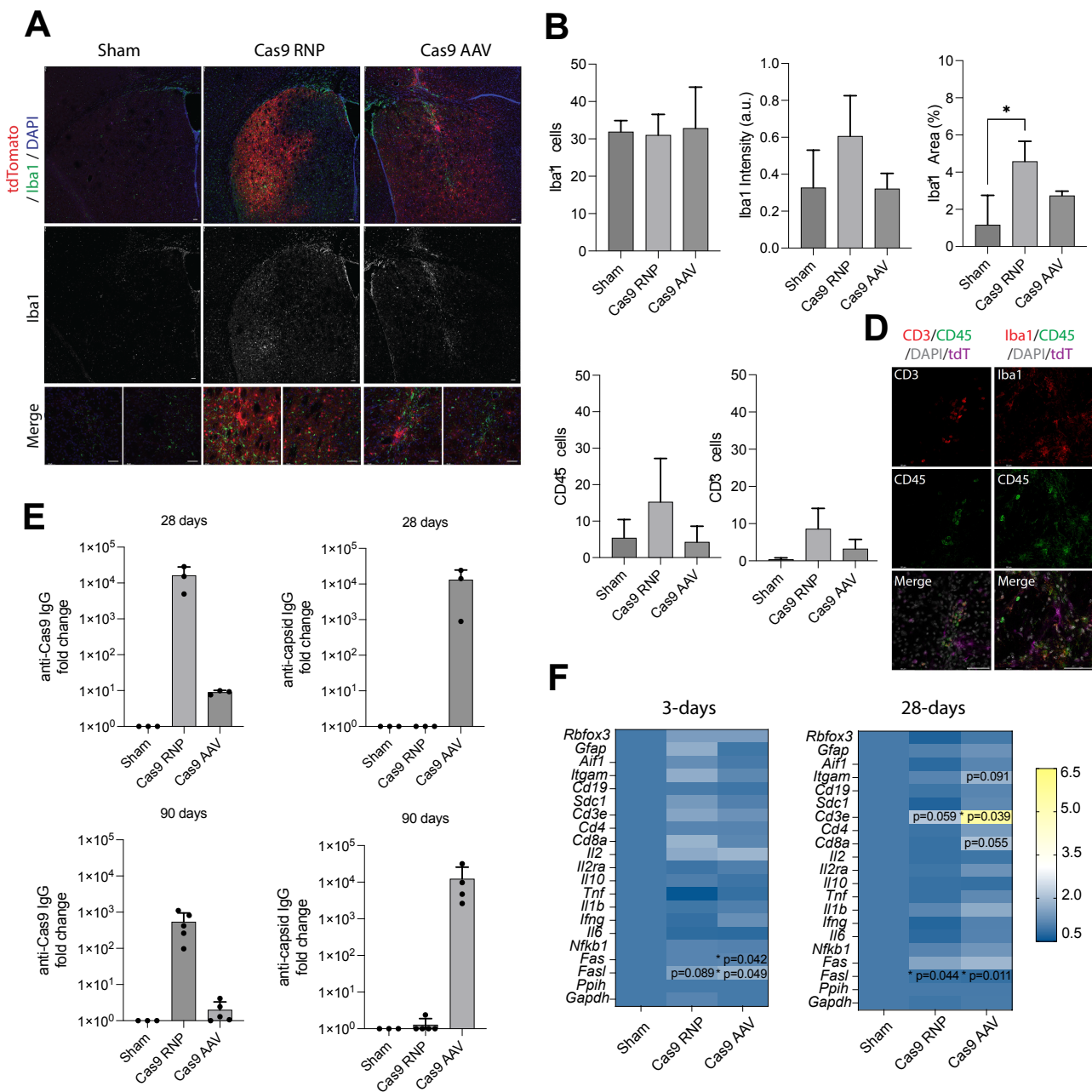


Figure 3. Optimized, low-endotoxin RNP formulation reduces local immune response

